MOLECULAR BIOLOGY

# Ribosome changes reprogram translation for chemosurvival in G0 leukemic cells

**Chandreyee Datta[1], Samuel S. Truesdell[1], Keith Q. Wu[1], Syed I. A. Bukhari[1], Harrison Ngue[1], Brienna Buchanan[1], Olivier Le Tonqueze[1], Sooncheol Lee[1], Swapna Kollu[1], Madeleine A. Granovetter[1]†, Myriam Boukhali[1], Johannes Kreuzer[1], Maheen S. Batool[2], Leonora Balaj[2], Wilhelm Haas[1], Shobha Vasudevan[1]***



**Quiescent leukemic cells survive chemotherapy, with translation changes. Our data reveal that FXR1, a protein amplified in several aggressive cancers, is elevated in quiescent and chemo-treated leukemic cells and promotes chemosurvival. This suggests undiscovered roles for this RNA- and ribosome-associated protein in chemosurvival. We find that FXR1 depletion reduces translation, with altered rRNAs, snoRNAs, and ribosomal proteins (RPs). FXR1 regulates factors that promote transcription and processing of ribosomal genes and snoRNAs. Ribosome changes in FXR1-overexpressing cells, including RPLP0/uL10 levels, activate eIF2α kinases. Accordingly, phospho-eIF2α increases, enabling selective translation of survival and immune regulators in FXR1-overexpressing cells. Overriding these genes or phospho-eIF2α with inhibitors reduces chemosurvival. Thus, elevated FXR1 in quiescent or chemo-treated leukemic cells alters ribosomes that trigger stress signals to redirect translation for chemosurvival.**

## INTRODUCTION

Cancer cells can enter a reversible arrest phase called quiescence or G0 that is resistant to harsh conditions including chemotherapy (*1*, *2*). We previously found that leukemic cells induced to G0 by growth factor deprivation not only are chemoresistant but also exhibit similar posttranscriptional changes, as that of leukemic cells surviving chemotherapy (*1*). This indicated translation of specific genes in these chemoresistant cells, which are needed for their chemosurvival. Understanding the altered translation program and how chemosurviving G0 cells translate specific genes can reveal undiscovered insights on chemoresistance and new strategies to reduce chemosurvival.

Canonical translation initiation is mediated by two rate-limiting steps: cap-dependent recruitment of mRNAs and recruitment of the initiator transfer RNA (tRNA)/ternary complex for translation initiation (*3*, *4*). This conventional translation promotes proliferation-associated genes (*5*). One of the two rate-limiting steps of canonical translation initiation is inhibited by dephosphorylation of the canonical cap complex inhibitor, EIF4EBP (4EBP), due to low mammalian Target of Rapamycin (mTOR) activity (*3*, *5*). The second rate-limiting step of canonical translation initiation is inhibited by phosphorylation of the tRNA recruitment complex factor, eIF2α. This is brought about by four eIF2α kinases (eIF2aks) that are triggered by various stress responses and cause the integrated stress response (ISR) (*4*, *6*). We found that eIF2α phosphorylation is enhanced in G0 and chemotherapy-treated cells (*1*), which can inhibit canonical translation at the tRNA recruitment step and enable specific genes to get translated. How G0 and chemotherapy-treated cells induce eIF2α phosphorylation, to suppress canonical translation and express specific genes that lead to chemosurvival and AML persistence, remains to be uncovered.

Our previous data revealed that the RNA binding protein, fragile X mental retardation–related protein 1 (FXR1) (*7*, *8*), is elevated in serum-starved G0 acute monocytic leukemic (AML) THP1 cells. FXR1 has been shown to be important for tumor progression as it is amplified in several aggressive cancers, where posttranscriptional expression of specific mRNAs is altered (*9*). FXR1 is associated with ribosomes, translation, mRNA stability, and export and localizes in the nucleus, cytoplasm, and stress granules (*7*, *8*). In serum-starved G0 cells, we found that FXR1a splice isoform is enhanced and can promote specific mRNA translation (*10*, *11*). Given that FXR1 increases and promotes specific mRNA translation in G0 AML cells (*10*, *11*) that are chemoresistant (*1*), the role of FXR1 on chemosurvival via translation mechanisms needs to be uncovered to understand the impact of translation regulation in refractory cancers.

In this study, we investigated the changes in translation, and the role of FXR1, in G0 and chemosurviving AML cells. Our findings demonstrate that as in serum-starved G0 cells that are chemoresistant, FXR1 increases in therapy-surviving AML cells. Consistently, we find that FXR1 depletion reduces chemosurvival, while FXR1 overexpression promotes chemosurvival. Our data reveal that FXR1 associates with ribosome regulators and alters ribosome components. These ribosomal changes trigger stress signaling via eIF2α kinase activation that causes eIF2α phosphorylation. This reduces canonical translation and permits translation of specific prosurvival and immune genes, leading to chemotherapy and immune survival. Pharmacological inhibition of this specific translation, or of translated prosurvival genes, suppresses chemosurvival, indicating new avenues to therapeutically target refractory AML.

## RESULTS

### FXR1 is elevated in cytarabine-treated, chemosurviving AML cells

We previously found that both serum-starved G0 THP1 AML cells where FXR1 increases (*10*) and chemosurviving AML cells show similar translation factor changes compared to untreated, proliferating AML [Fig. 1, A and B, mass spectrometry data (*1*)]—which may

[1]Massachusetts General Hospital Cancer Center, Department of Medicine, Harvard Medical School, Boston, MA 02114, USA. [2]Department of Neurosurgery, Massachusetts General Hospital, Harvard Medical School, Boston, MA 02114, USA.
*Corresponding author. Email: vasudevan.shobha@mgh.harvard.edu
†Present address: Robert Wood Johnson Medical School, Rutgers University, New Brunswick, NJ 08901, USA.

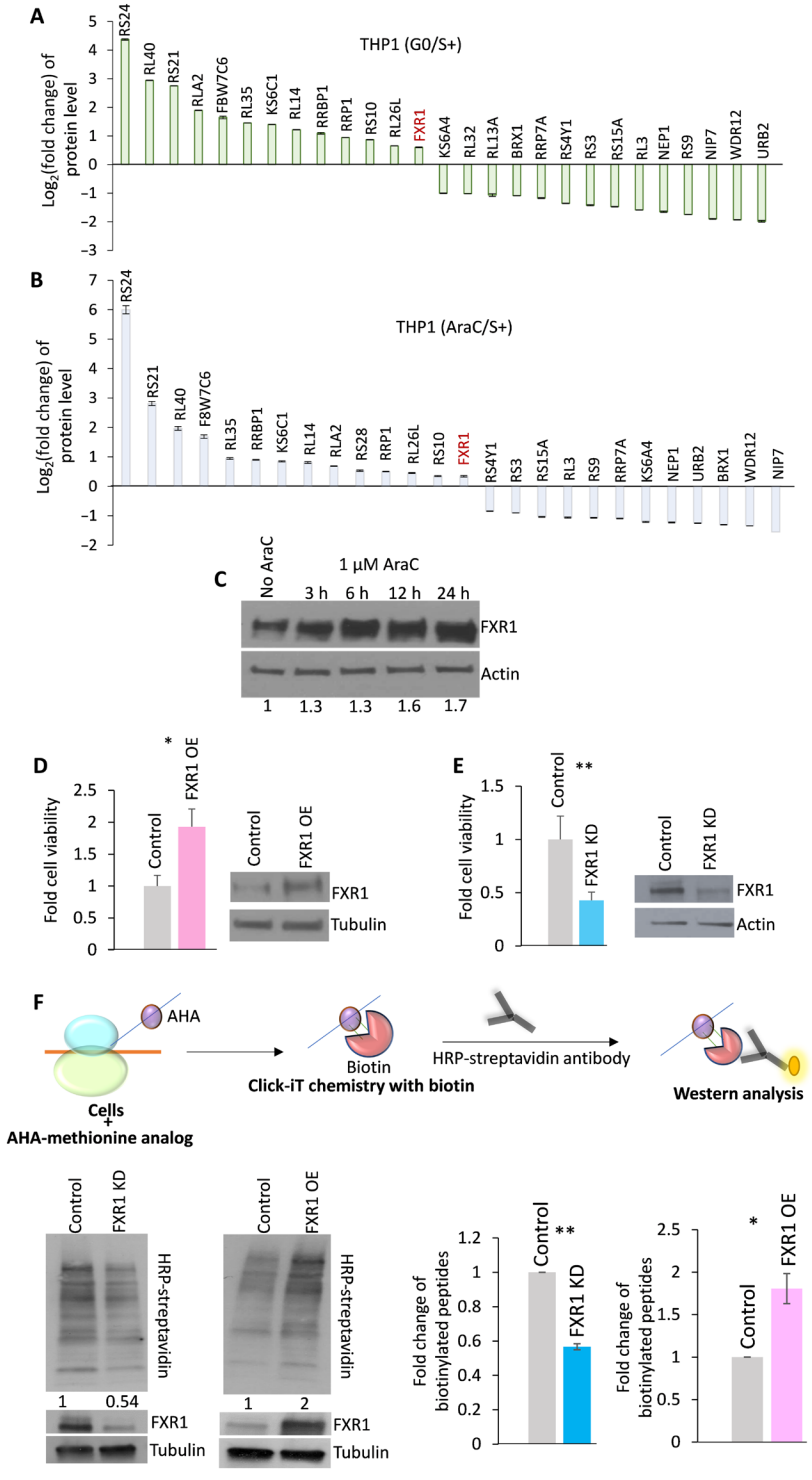


**Fig. 1. FXR1 is required for translation.** (**A** and **B**) Graphs showing proteomic levels [TMT spectrometry from (*1*)] of commonly up-regulated RPs and regulators including the RNA- and ribosome-associated regulator, FXR1. (A) THP1 cells grown in serum-starved medium (G0) for 4 days. (B) THP1 cells treated with cytarabine (AraC) at 5 μM [within clinical range (*12*, *13*)] for 3 days, as conducted previously (*1*). (**C**) FXR1 levels over time of AraC (1 μM) treatment. FXR1 runs as multiple bands that include posttranslational modifications and splice isoforms (*7*, *8*). (**D** and **E**) AraC survival after 24-hour treatment, observed by trypan blue stain exclusion cell counts, (D) in FXR1 overexpression (FXR1 OE) compared to control vector, and (E) in FXR1 knockdown (FXR1 KD) compared to control shRNA cells; Western blot below of FXR1, with tubulin and actin as loading controls. (**F**) Comparison of global translation by labeling nascently translated proteins in FXR1 KD compared to shRNA control cells, and in FXR1 OE compared to control vector cells, with L-homopropargylglycine (HPG), an amino acid analog of methionine containing an alkyne moiety that is biotinylated by Click-iT chemistry (Thermo Fisher Scientific), followed by SDS-PAGE and HRP-streptavidin Western analysis; Western analysis of FXR1 levels below and quantification of labeled protein levels on the right. Data are average of three replicates ± SEM. See also fig. S1.

underlie their common ability to survive chemotherapy (*1*). Therefore, we asked the question whether FXR1, an RNA and translation regulator, could be amplified in chemotherapy-treated cells. We tested FXR1 levels by Western blot analysis in cytarabine (AraC) chemotherapy-treated cells (*1*) at clinically relevant concentrations (*12*, *13*). We find that FXR1 is transiently elevated in AraC-treated THP1 cells (AraC; Fig. 1C and fig. S1A), as in serum-starved G0 cells (*10*) that are chemoresistant (*1*). This was also observed upon AraC treatment of another AML cell line, NOMO1 (fig. S1B), indicating that FXR1 elevation upon AraC treatment was not unique to THP1 cells. These data reveal transient elevation of FXR1 levels upon AraC therapy treatment in AML.

### THP1 cell survival, upon treatment with AraC chemotherapy, is promoted by FXR1 overexpression and reduced by FXR1 depletion

To investigate whether FXR1 plays a role in chemosurvival of G0 and AraC-treated cells where it is elevated, we used a previously constructed THP1 cell line for FXR1 depletion (*10*, *11*). This is stably transduced with a doxycycline-inducible short hairpin RNA (shRNA) lentiviral vector (FXR1 KD), compared to a parallel control shRNA-expressing cell line. These cells are induced with doxycycline to express the shRNA for 3 days to effectively deplete all FXR1 isoforms (*10*, *11*). We previously observed that FXR1a isoform increases in G0 THP1 cells (*10*). Therefore, we also constructed a THP1 cell line that constitutively overexpresses FXR1a (FXR1 OE) compared to a control vector cell line. Western blot analysis shows that FXR1 was effectively depleted or overexpressed (Fig. 1, D and E, Western blots). These were treated with AraC for 24 hours to test the impact of FXR1 levels on chemosurvival. Consistent with its increase in AraC-surviving cells, we find that FXR1 overexpression promotes chemosurvival by 1.9-fold, while FXR1 depletion reduces chemosurvival to less than 50% (Fig. 1, D and E, graphs). These data suggest that FXR1 promotes chemosurvival of THP1 cells.

### FXR1 depletion decreases, while overexpression promotes, translation

We next explored the mechanism of how FXR1 may promote chemosurvival. To investigate the effect of FXR1 on translation, we performed nascent translation labeling analysis in FXR1 KD compared to control shRNA cells and in FXR1 OE compared to vector control cells. We used L-homopropargylglycine (HPG), an amino acid analog of methionine containing an alkyne moiety that can be biotinylated by Click-iT chemistry (Thermo Fisher Scientific), for labeling nascently translated proteins, followed by SDS–polyacrylamide gel electrophoresis (SDS-PAGE) and horseradish peroxidase (HRP)–streptavidin Western analysis and quantification. We verified this by $^{35}$S-Met incorporation (*14*) to label nascently translated proteins in FXR1 KD cells followed by SDS-PAGE. We find that FXR1 depletion decreases protein synthesis by almost half, compared to control shRNA cells (Fig. 1F and fig. S1C). Conversely, FXR1a overexpression increases nascent translation by 1.7-fold compared to control vector cells (Fig. 1F). These data suggest that FXR1 is needed for translation.

### FXR1 depletion decreases, while overexpression increases, ribosomal RNAs

Given the decrease in global translation, we investigated whether FXR1 levels alter ribosome biogenesis. Ribosome biogenesis includes ribosomal RNA (rRNA) transcription and processing, rRNA modification, and ribosomal proteins (RPs) and their assembly, mediated by several regulators (*15*–*18*). Analysis of rRNAs by quantitative polymerase chain reaction (qPCR) and droplet digital PCR (ddPCR) revealed a significant decrease in 28*S*, 18*S*, and 5.8*S* rRNAs upon FXR1 depletion, compared to control shRNA cells (Fig. 2A and fig. S2A). Conversely, 28*S*, 18*S*, and 5.8*S* rRNAs increase upon FXR1 overexpression compared to control vector cells. FXR1 depletion also reduces, while overexpression increased, the RNA Polymerase I (Pol I) rRNA precursor 45*S* rRNA (Fig. 2A), indicating that ribosome gene transcription and processing are affected by FXR1. Apart from Pol I–derived 28*S*, 18*S*, and 5.8*S* rRNAs, the fourth Pol III–transcribed 5*S* rRNA is also decreased and enhanced with FXR1 (Fig. 2A), suggesting that FXR1 may be altering a common Pol I and Pol III regulator and/or multiple ribosome biogenesis regulators. These data are consistent with decreased translation in FXR1 KD cells and enhanced translation in FXR1 OE cells (Fig. 1F) and suggest that FXR1 levels affect ribosome biogenesis.

### Specific snoRNAs, involved in rRNA processing and modification, are elevated in G0 or FXR1-overexpressing cells and decrease upon FXR1 depletion

Ribosome biogenesis involves RNA regulators called small nucleolar RNAs (snoRNAs) that process or modify rRNAs. SnoRNAs involved in rRNA processing, such as U3 (snoRD3) and U8 (snoRD118), bind RNA-protein complexes (RNPs) that are required to cleave and process the 47*S* rRNA precursor into mature 18*S*, 28*S*, and 5.8*S* rRNAs. Other snoRNAs bind modification enzymes and RNA binding proteins to form snoRNPs that are known to base pair and modify rRNAs at specific sites. Box C/D snoRNAs (snoRD) recruit fibrillarin enzyme to cause 2′-*O*-methylation, while Box H/ACA snoRNAs (snoRA) recruit Dyskerin enzyme to pseudo-uridylate rRNA sites. These modifications affect ribosome interactions and are important for translation (*16*, *19*–*22*).

We first examined levels of snoRNAs involved in rRNA cleavage, U3 and U8. RNA profiling in G0 and proliferating cells revealed that U3 (snoRD3) increases in G0 cells (table S1, A to C) (*1*, *10*, *11*). Consistently, qPCR analysis reveals that U3 and U8 decrease upon FXR1 depletion and are enhanced upon FXR1 overexpression (Fig. 2B and fig. S2A), which can affect 45*S*, 28*S*, 18*S*, and 5.8*S* rRNA levels in Fig. 2A. Profiling also revealed that several snoRNAs that modify distinct rRNA sites are elevated in G0 compared to proliferating cells (table S1, A to C) and decrease in RNA profiles of FXR1 KD cells compared to control shRNA cells (Fig. 2C and table S1, A to C). These data are consistent with the impact of FXR1 observed on translation and rRNA levels (Figs. 1F and 2A).

### SnoRNAs regulated by FXR1 alter rRNA modification

To test the outcome of FXR1 regulation of snoRNA levels, we analyzed FXR1 KD or OE cells for 2′-*O*-methylation [by low deoxynucleotide triphosphate (dNTP) reverse transcription qPCR (RT-qPCR)] and pseudouridylation [after *N*-cyclohexyl-*N*′-(2-morpholinoethyl) carbodiimide metho-*p*-toluenesulfonate (CMC metho-*p*-toluene sulfonate) treatment followed by low dNTP RT-qPCR (*21*, *23*, *24*)] at the rRNA sites of specific snoRNAs that increase in G0 cells but decrease in G0 FXR1 KD cells (table S1, A to C). To globally examine rRNA modification changes, with or without FXR1, we enriched rRNA [devoid of poly(A) RNA and RNAs fractionated, to remove tRNAs and other RNAs less than 200 nucleotides (nt)] from FXR1 KD G0 and control shRNA G0 cells and subjected the nucleosides to liquid chromatography–mass spectrometry (LC-MS) analysis (fig. S2B and table S1D).

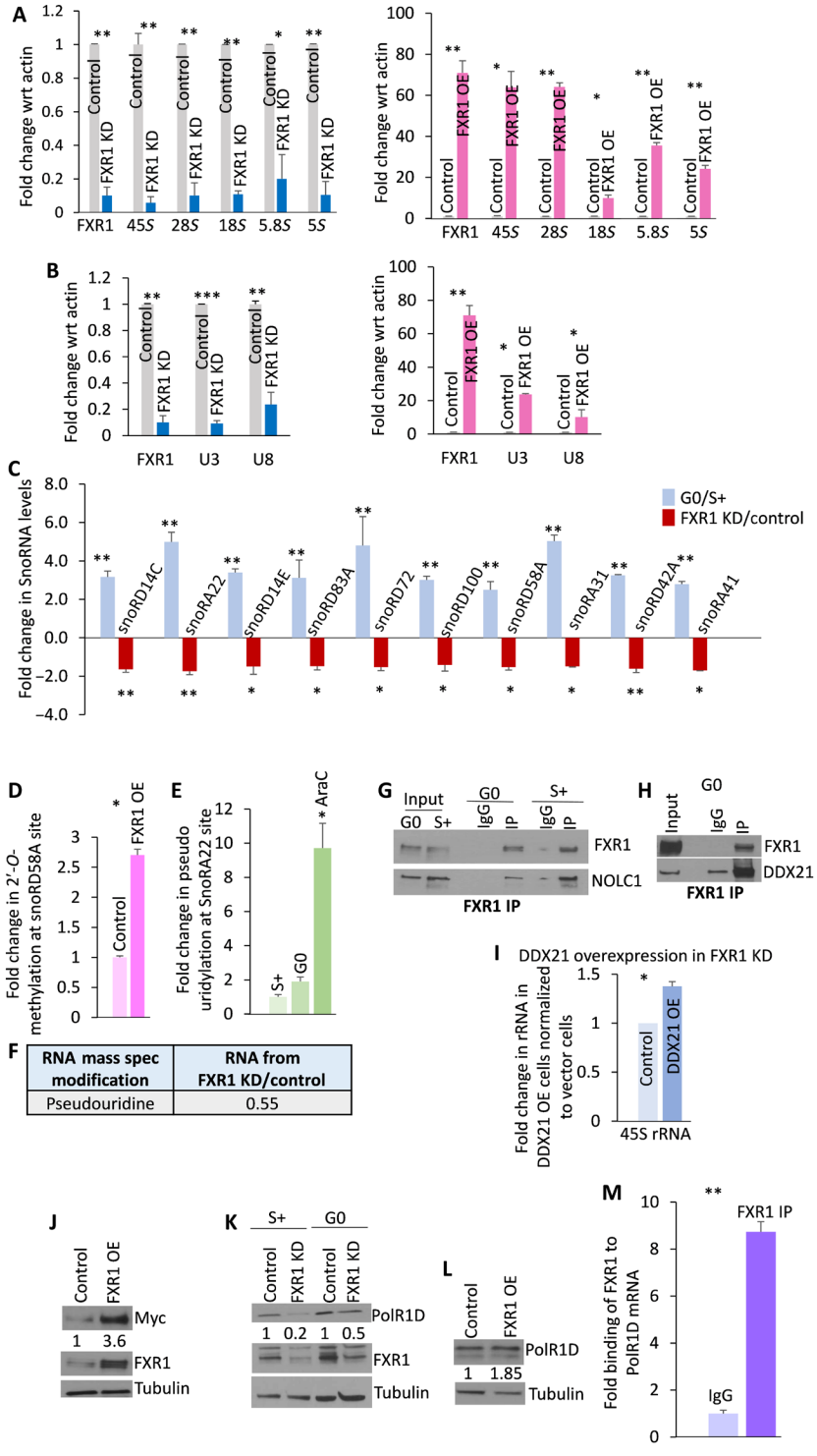


**Fig. 2. FXR1 regulates rRNAs and snoRNAs and associates with ribosome and snoRNA regulators.** qPCR of rRNAs and snoRNAs normalized to actin mRNA: (**A**) 45*S*, 18*S*, 28*S*, 5.8*S*, and 5*S*; (**B**) snoRNAs U3 and U8 in FXR1 KD compared to control cells and in FXR1-OE compared to control cells. (**C**) SnoRNAs from normalized microarray profiles in FXR1 KD G0 cells compared to control cells (red) and G0 cells compared to proliferating cells (blue) (table S1, A to C). (**D**) 2′-*O*-methylation assay by low dNTP RT-qPCR, in FXR1-OE cells compared to control cells, of 28*S* rRNA site (G4198m) modified by snoRD58A (table S1, A to C). (**E**) Pseudouridylation of 28*S* rRNA (U4966 and U4975) by snoRA22 (table S1, A to C), in AraC-treated, G0, and S+ cells, measured by CMC treatment followed by low dNTP RT-qPCR. (**F**) Mass spectrometry of pseudouridine in rRNA from G0 FXR1 KD compared to control cells (table S1D). In vivo formaldehyde crosslinking-coupled FXR1 immunoprecipitation followed by Western blots of FXR1, (**G**) NOLC1, (**H**) DDX21, and (**I**) qPCR of partial rescue of 45*S* rRNA by DDX21 overexpression in FXR1 KD cells. (**J**) Western blots of c-MYC in FXR1-OE versus control cells. Western blots of POLR1D in (**K**) FXR1 KD G0 and S+ cells and (**L**) FXR1-OE versus control cells. (**M**) qPCR for PolR1D mRNA in FXR1 immunoprecipitates compared to IgG from in vivo–crosslinked G0 cells. Data are average of three replicates ± SEM. See also fig. S2 and tables S1 and S2.

Our data show changes in modification at rRNA sites targeted by the snoRNAs that are increased in G0 and regulated by FXR1. As shown in Fig. 2D, the target modification site on 28*S* rRNA (G4198m) of the box C/D (2′-*O*-methylation eliciting, fibrillarin-bound) snoRNA, snoRD58A, shows enhanced 2′-*O*-methylation in FXR1 OE cells, consistent with snoRD58A elevation in G0 cells where FXR1 increases, and its decrease in FXR1 KD cells (Fig. 2C). snoRA22 is a H/ACA Dyskerin-bound snoRNA that causes pseudouridylation, which is elevated in G0 (table S1, A to C); in accord, rRNA pseudouridylation at snoRA22 target sites on 28*S* rRNA (U4966, U4975) is enhanced in AraC-treated cells (Fig. 2E). Consistent with the decrease of snoRA22 and other such pseudouridylation-causing, Dyskerin-associated, H/ACA snoRNAs, upon FXR1 depletion (table S1, A to C), we find that FXR1 knockdown reduces rRNA pseudouridylation by mass spectrometry, along with alterations in other known rRNA modifications (Fig. 2F, fig. S2B, and table S1D). The rRNA sites targeted by these FXR1-regulated snoRNAs can affect tRNA interaction and translation (*25*–*29*). These data suggest that FXR1 regulates levels of specific snoRNAs in G0, which can affect rRNA levels and modifications, to alter translation in these chemosurviving cells.

### FXR1 interacts with rRNA and snoRNA regulators and modulates the levels of ribosome gene transcription factors

To identify how FXR1 affects snoRNAs and rRNAs, we examined FXR1-interacting regulators by in vivo crosslinking G0 cells followed by FXR1 immunoprecipitation and tandem mass tag (TMT) spectrometric analysis (*10*) of coimmunoprecipitates (table S2). We find that FXR1 interacts with multiple ribosome- and translation-related proteins in G0 (fig. S2C). In vivo crosslinking-coupled FXR1 immunoprecipitation in control or FXR1 OE cells reveals FXR1 association with rRNAs (fig. S2D). These data suggest that FXR1 may interact with ribosome regulators.

We find that snoRNA and ribosome regulators, NOLC1 and DDX21, coimmunoprecipitated with FXR1 (Fig. 2, G and H; fig. S2C; and table S2), indicating that FXR1 may affect ribosome levels through interactions with these ribosome regulators. NOLC1 is a snoRNA and ribosome regulator that is involved in their assembly and biogenesis (*30*, *31*). DDX21 (*32*, *33*) binds and affects the roles of snoRNAs that control rRNA modification and processing. DDX21 also promotes ribosome transcription via Pol I for rRNAs and Pol II for snoRNA and RP expression (*34*). Consistently, DDX21 overexpression in FXR1 KD cells, where rRNA levels decrease (Fig. 2A), partially rescued the rRNA defect by increasing 45*S* rRNA levels (Fig. 2I).

In addition, FXR1 has been recently shown to bind and regulate the 3′ untranslated region (UTR) of c-MYC mRNA (*35*), a major ribosome gene transcription regulator that affects all three polymerases and regulates ribosome biogenesis (*36*). Consistently, we find that c-MYC increases upon FXR1 overexpression (Fig. 2J), which could lead to enhanced ribosome biogenesis. Since FXR1 affects both Pol I transcript 45*S* rRNA and Pol III transcript 5*S* rRNA (Fig. 2A), we hypothesized that a common component of both Pol I and Pol III complexes may be affected by FXR1 and G0 chemoresistant cell conditions, leading to this coordinated impact on both Pol I– and Pol and Pol III components are increased in G0 and are affected in FXR1-depleted or FXR1-overexpressed cells. POLR1D is an essential component of both Pol I and Pol III complexes and is needed for DDX21 to locate to the nucleolus (*32*, *34*); thus, POLR1D can affect 45*S* and 5*S* rRNAs, and DDX21 functions on snoRNAs, Pol I, and Pol II. Mass spectrometry dataset from G0 and AraC-treated cells reveals that POLR1D increases in G0 and AraC-treated cells (table S3A) but is reduced upon FXR1 depletion (fig. S2E and table S3, A to D, sheet d). Consistently, we find that POLR1D is reduced and overexpressed with FXR1 knockdown or overexpression, respectively (Fig. 2, K and L). Accordingly, we find that POLR1D mRNA binds FXR1 (Fig. 2M), indicating that FXR1 associates with POLR1D mRNA to modulate levels of this rRNA transcription regulator. These data suggest that FXR1 interacts with or regulates levels of multiple ribosome biogenesis factors to alter ribosomes in G0 and AraC-treated cells where FXR1 is elevated.

### RP levels are altered in G0 cells, AraC-treated cells, and FXR1-overexpressing cells

SnoRNAs, rRNAs, and their regulators are modulated by FXR1 that increases in G0 and AraC-treated cells, where RPs and regulators are also altered (Figs. 1, A and B, and 2 and table S3, A to H). Many RPs modulate rRNA processing (*16*–*18*), and RP genes are regulated transcriptionally by DDX21 and c-MYC that are modulated by FXR1 (Fig. 2, H to J, and tables S1 and S3, A to G). In addition, we find that some RPs interact with FXR1 in G0 (fig. S2C and table S2), consistent with previous studies that showed that RPs interact with FXR1 (*7*). FXR1 amplification in G0 and AraC-treated cells could alter RPs to elicit changes in ribosome complexes (*37*) and translation output; therefore, we examined RPs upon FXR1 depletion and overexpression.

We find that a specific set of RPs are commonly increased or decreased, in both serum-starved G0 and AraC-treated cells in proteomic analyses [Fig. 1, A and B, and table S3B; TMT mass spectrometry G0 and AraC data from table S3A (*1*)], indicating that common changes in RP composition occur in these chemoresistant cells. Some RPs that increase in G0 and AraC (table S3B; TMT mass spectrometry G0 and AraC) decrease upon FXR1 depletion (FXR1 KD cells compared to control shRNA cells) or are enhanced upon FXR1 overexpression (FXR1 OE cells compared to control vector cells), as seen by qPCR (Fig. 3A, RPL8 and RPS14), Western blot (Fig. 3, B to D, RPLP0, P2, L19, and L29), or profiling analyses [fig. S3A and table S3, C, E, and G: RNA profiling data in FXR1 KD compared to control shRNA cells in table S3C from table S1A, proteomic data of FXR1 KD compared to control shRNA cells in table S3D, and translatome data from FXR1 KD compared to control shRNA cells in table S3G from table S3F (*10*, *11*)]. These data suggest ribosome changes in cells with elevated FXR1 levels, as in G0 and AraC-treated cells, which can affect ribosome complexes and translation.

### Distinct ribosome complexes are observed in G0 or AraC-treated cells, compared to proliferating, untreated cells, but are similar to ribosome complexes in FXR1-overexpressing cells

As rRNA processing, RP level, and modification changes are induced in G0 by FXR1 overexpression (Figs. 2 and 3, A to D), we analyzed ribosome complexes formed in AraC-treated and serum-starved G0 cells to test whether they are distinct compared to proliferating cells. We also compared these with ribosome complexes in FXR1-overexpressing cells compared to control vector cells, as they show similar chemosurvival and ribosome changes to G0 and AraC-treated cells. These cells were first subject to formaldehyde crosslinking to freeze in vivo complexes. Cytoplasmic extracts were prepared to avoid nuclear, preribosome complexes that are not assembled. To identify changes in ribosome complexes, the extracts were bound on an anionic diethylaminoethanol

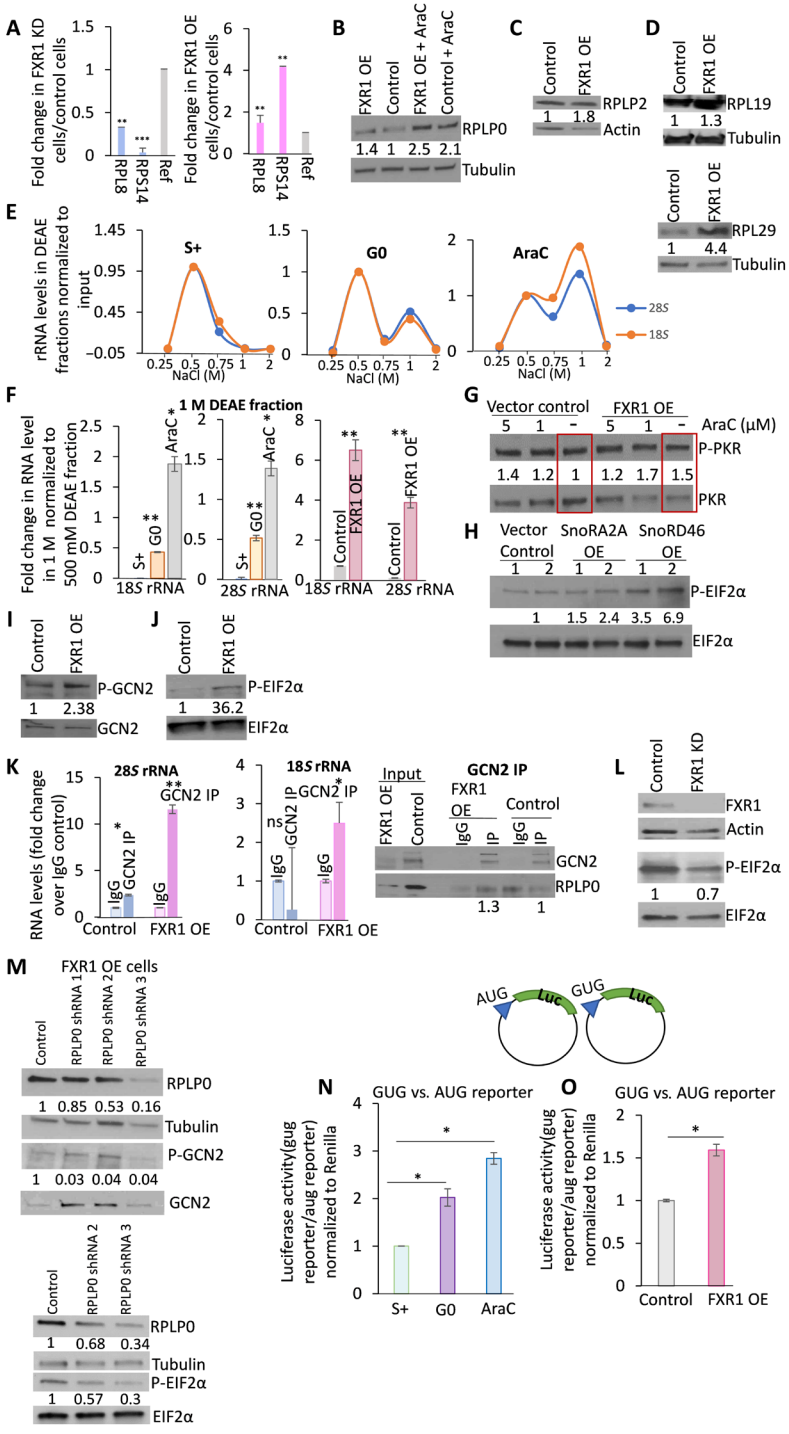


**Fig. 3. eIF2α phosphorylation and noncanonical start site translation increase with altered ribosomal components upon FXR1 overexpression.** (**A**) RP levels by qPCR normalized to actin mRNA in FXR1 KD and in FXR1-OE compared to control cells (table S3C). Western blots of (**B**) RPLP0, (**C**) RPLP2, and (**D**) RPL19 and RPL29 in FXR1-OE and control cells. (**E**) Y10B immunoprecipitation from in vivo–crosslinked cytoplasmic extracts, followed by DEAE fractionation to analyze ribosome complex migration in salt fractions in G0 and AraC-treated cells compared to S+ cells by qPCR for 18*S* and 28*S* rRNAs (representing 80*S* ribosomes) comigration. (**F**) DEAE fractionation and qPCR of rRNAs of Y10B-immunopurified ribosome complexes (18*S*, 28*S* rRNAs) in the 1 M fraction normalized to 500 mM fraction, from G0, and AraC-treated cells, versus S+ cells; FXR1-OE cells versus control cells. (**G**) Western blots of phospho-PKR in FXR1-OE, AraC-treated versus control cells. (**H**) snoRA2A and snoRD46 overexpression, followed by Western blot for phospho-eIF2α. Western blot of (**I**) phospho-GCN2 and (**J**) phospho-eIF2α in FXR1-OE versus control cells. (**K**) GCN2 immunoprecipitation, followed by rRNA qPCR; Western blot of RPLP0 and GCN2 (In = 10% input), in FXR1-OE versus control cells. (**L**) Western blot of phospho-eIF2α in FXR1 KD versus control cells. (**M**) Western blot of phospho-GCN2 and phospho-eIF2α in FXR1-OE cells transfected with control or RPLP0 shRNAs. (**N**) Translation ratios of GUG start site luciferase over AUG reporter normalized to cotransfection Renilla. G0, AraC-treated compared to S+ cells. (**O**) FXR1-OE compared to control cells. Data are average of three replicates ± SEM. See also fig. S3 and table S3.

(DEAE) column and eluted by increasing salt concentrations to separate complexes (*10*). Fractions of the in vivo crosslinked complexes that contained both 18*S* and 28*S* rRNAs, depicting small and large subunits, were examined as composite 80*S* ribosome complexes. We observed one peak at 500 mM salt in untreated, serum-grown cells; in contrast, we find a second distinct peak (1 M salt) of ribosome complexes in G0 and AraC-treated cells (fig. S3B). Strikingly, we observed similar two peaks, eluting in the same salt fractions (500 mM, 1 M), in FXR1-overexpressing cells compared to one (500 mM) in vector control cells (fig. S3B). These data suggest changes in ribosome complexes that could affect translation and chemosurvival that is commonly observed in G0, AraC-treated, and FXR1-overexpressing cells, but not in untreated, control vector cells (Figs. 1 and 2).

We wanted to ensure that these complexes separated on DEAE are enriched for ribosomes. Therefore, we immunopurified ribosomes from G0 and AraC-treated cells compared to untreated, serum-grown cells, as well as FXR1-overexpressing cells compared to control vector cells, and then examined them by DEAE fractionation. These cells were first subject to formaldehyde crosslinking to freeze in vivo ribosome complexes. Ribosome complexes were purified from cytoplasmic extracts (to avoid nuclear, preribosome complexes) by Y10B, an antibody that recognizes 5.8*S* complexes in assembled 80*S* complexes (fig. S3C) (*38*). Y10B immunopurification of assembled 80*S* ribosomes was verified by qPCR analysis of enrichment of 5.8*S* rRNA and Western analysis of ribosomal protein RPLP0 in Y10B immunoprecipitates compared to immunoglobulin G (IgG) control (fig. S3, D and E). Lack of unprocessed 45*S* rRNA in Y10B immunoprecipitates verified the absence of partially processed, nuclear preribosomes in Y10B immunoprecipitates of 80*S* cytoplasmic ribosome complexes (fig. S3D). To test whether Y10B-purified ribosome complexes migrate distinctly in G0, AraC-treated, and FXR1-overexpressing cells, compared to control vector or untreated, serum-grown cells, the Y10B immunoprecipitates were fractionated over DEAE and eluted with increasing salt. These were examined for fractions that showed both 18*S* and 28*S* rRNAs depicting small and large subunit rRNAs, as composite 80*S* ribosome complexes, by qPCR analysis. While untreated, serum-grown cells showed a single peak at 500 mM salt, a second complex is observed at 1 M salt in G0 and AraC-treated cells (Fig. 3, E and F), consistent with the ribosome component changes observed in these conditions in Figs. 2 and 3 (A to D) and in fig. S3B. We observe a similar pattern of two distinct peaks of ribosome complexes seen in G0 and AraC-treated cells, eluting in the same salt fractions (500 mM, 1 M) in FXR1-overexpressing cells compared to the single lower salt peak in control vector cells (Fig. 3F). These data suggest that in FXR1 overexpression conditions that include exogenously overexpressed, G0, and AraC-treated cells, ribosomal complex changes are observed. While distinct RNPs associated with the ribosome, or partially formed 80S could cause altered complex migration, these data suggest that ribosomes are differentially bound or comprised in FXR1-overexpressing cells and migrate in fractions that are similarly observed in G0 and AraC-treated cells, but not in untreated, proliferating cells.

### Altered P stalk proteins and snoRNAs in G0 cells, AraC-treated cells, and FXR1-overexpressing cells enhance eIF2α phosphorylation

These multiple changes on the ribosome can alter many downstream mechanisms to affect translation; one way is by activating stress signaling pathways (*39*–*42*). G0 and AraC-surviving cells where FXR1 increases show inhibition of canonical translation with increased phosphorylation of eIF2α (*1*). This is brought about by eIF2α kinases that respond to multiple stress signals and can be induced by ribosomal component changes elicited by increased FXR1: via enhanced snoRNAs (*43*, *44*) and via ribosome changes in the P stalk RPs (*39*, *40*).

FXR1 enhances levels of several snoRNAs (table S1, A to C) that have been shown to bind RNA-activated protein kinase (PKR) eIF2α kinase (eIF2ak2), a double-stranded RNA (dsRNA) binding protein (*43*, *44*) that causes eIF2α phosphorylation. We hypothesized that increased snoRNAs by FXR1 amplification, as in G0 and AraC-treated cells, could, in part, lead to eIF2α phosphorylation, as snoRNAs have been shown to activate eIF2ak2 or PKR (*43*, *44*). Consistently, we find that FXR1-overexpressing cells and AraC-treated cells show increased phosphorylation and thus activation of PKR (Fig. 3G). Therefore, we tested the impact on eIF2α phosphorylation upon overexpression of two snoRNAs that are enhanced in G0 cells, snoRD46 and snoRA2A. We verified overexpression of these transfected snoRNAs by qPCR compared to a control vector (fig. S3F). We find that overexpression of these snoRNAs leads to elevated eIF2α phosphorylation, compared to expression of a control vector (Fig. 3H). This suggests that overexpression of FXR1 alters snoRNAs, which can activate PKR (*43*, *44*) and phosphorylate eIF2α.

Recent studies also show that P stalk proteins, RPLP2, RPLP1, and RPLP0 or uL10, promote phosphorylation of eIF2α by activation of GCN2 eIF2α kinase (eIF2ak4), via RPLP0 interaction (*39*, *40*). Significantly, we find that RPLP0 increases in FXR1-overexpressing cells (Fig. 3B) and decreases upon FXR1 knockdown (fig. S3A and table S3C). Similarly, we find RPLP2 elevated in FXR1-overexpressing cells (Fig. 3C). Consistent with studies that demonstrated that P stalk proteins can interact with and activate GCN2 and cause eIF2α phosphorylation (*39*, *40*), we tested FXR1-overexpressing cells for GCN2 phosphorylation that marks its activation and for downstream eIF2α phosphorylation. We find that FXR1-overexpressing cells—where RPLP0 is enhanced, as in AraC-treated cells (Fig. 3B)—show increased GCN2 phosphorylation (Fig. 3I) and concordantly enhanced eIF2α phosphorylation (Fig. 3J). Concurrently, we find that GCN2 associates more significantly with ribosomes and RPLP0 in FXR1-overexpressing cells (Fig. 3K), which may enable GCN2 activation and eIF2α phosphorylation (*39*, *40*). Conversely, eIF2α phosphorylation decreases upon FXR1 depletion in THP1 and other cell types (Fig. 3L and fig. S3G). This increase in FXR1 and eIF2α phosphorylation is regulated over time of AraC treatment but is variable at higher concentrations of AraC (fig. S3, H and I), likely due to multiple effects including cell death and feedback regulation of phosphatases and mTOR that affect eIF2α phosphorylation and FXR1 levels (*1*, *10*, *45*). GCN2 phosphorylation and activation, and eIF2α phosphorylation in FXR1-overexpressing cells, is reduced upon RPLP0 knockdown (Fig. 3M), consistent with the need for RPLP0 in FXR1 overexpression conditions for GCN2 activation and eIF2α phosphorylation. These data suggest that ribosome changes in FXR1-overexpressing cells, as in G0 and AraC-treated cells, elicit eIF2α phosphorylation.

### FXR1-overexpressing cells, similar to G0 and AraC-treated cells, promote translation of noncanonical start sites

eIF2α phosphorylation inhibits canonical translation and reduces the stringency of selecting canonical AUG start sites that are present within a strong Kozak consensus sequence. This permits unconventional translation, including use of mRNAs with structured 5′UTRs, start sites in poor Kozak consensus, or non-AUG start sites (*3*, *46*–*48*).

FXR1 amplification in G0, AraC-treated, and FXR1 OE cells leads to multiple ribosome alterations (Figs. 2 and 3, A to F). Increased snoRNA modification can promote noncanonical translation (*24*), while altered ribosomes can promote specific mRNA 5′UTR translation (*37*), and eIF2α phosphorylation can inhibit canonical translation to permit translation of specific 5′UTRs and noncanonical start sites (*47*). As these changes, upon FXR1 elevation in G0 and AraC-treated cells, can redirect translation, we tested whether luciferase reporters with a noncanonical GUG start site would be translationally up-regulated, over a canonical AUG start site reporter. We normalized both these reporters to a Renilla reporter as cotransfection control and for RNA levels.

In G0 and AraC-surviving cells, we find that the translation of GUG reporter over that of the AUG reporter is enhanced, compared to the translation ratio in untreated, serum-grown proliferating cells (Fig. 3N), indicating that translation of unconventional start sites is enabled in G0 and AraC-treated conditions. We tested whether FXR1 overexpression affects translation of noncanonical start sites, as this translation could be due to FXR1 amplification, or other factors in G0 and AraC-treated cells. We find that, as in G0 cells, the translation of GUG reporter over that of the AUG reporter is enhanced in FXR1-overexpressing cells, compared to control vector cells, even without induction of G0 or AraC treatment (Fig. 3O). These changes in luciferase expression are not seen at the RNA level (fig. S3J). These data suggest that translation of atypical start sites is enabled in G0 cells, AraC-treated cells, and FXR1 OE cells.

### FXR1 overexpression promotes translation of survival genes

The above data suggested that FXR1 overexpression in G0 and AraC-treated cells may promote translation of specific mRNAs. To identify which mRNAs are translated because of FXR1 amplification seen in G0 and AraC-surviving cells but without G0 or AraC conditions that could induce other effectors, we conducted polysome profiling of control vector and FXR1 OE cells without G0 or AraC treatment (Fig. 4A). The heavy polysomes (>2) were pooled and profiled by microarray compared to input samples to identify mRNAs that are promoted or repressed on polysomes by FXR1 overexpression (table S4, A and B). We find that ~10% [312 (AraC-treated proteome; table S3A) to 407 (G0 proteome; table S3A) genes of 3575 genes above 1.3-fold in table S4A shown in table S4C] are genes that are commonly up-regulated in FXR1 overexpression translatome (table S4, A to C) and in the proteome of AraC-treated and G0 cells (table S3A). Many of these proteins are also known to be increased in G0 but decreased upon FXR1 depletion from our datasets (table S3) (*1*, *10*). Apart from prosurvival oncoproteins like BCL6 (*49*) and antitumor immune regulators such as CD47 (*50*) that we previously noted to be up-regulated in G0 and AraC-treated cells (*1*) (Fig. 4B and tables S3A and S4, A to D), mRNAs translated upon FXR1 overexpression also include stress response genes like XBP1 (*51*), cell adhesion genes like PECAM1 (*52*), signaling regulators that include phosphatidylinositol 3-kinase (PI3K)–AKT–mTOR pathway (*45*), and metabolic enzymes like PDK3 (*53*) that are known to promote tumor survival (Fig. 4B and table S4, A to D).

In addition, several classes of critical genes such as immune cell receptors that would be recognized by immune cells, and immune cell–attracting chemokines, are decreased in the translatome of FXR1-overexpressing cells compared to control vector cells (Fig. 4B, down in translatome genes, and table S4E). The suppression of immune recognition receptors and chemokines, while inducing immune evasion receptors like CD47, suggests specific mRNA translation to survive antitumor immunity. These data suggest that specific gene categories are modulated by FXR1 increase to enable AML survival.

### Specific mRNA translation in G0 cells with distinct 5′UTRs

To verify the translationally up-regulated mRNAs in FXR1 OE cells in table S4 (A to D), we performed qPCR analysis of polysome fractions that are normalized for input levels, which reveal that these mRNAs are enriched on polysomes of FXR1 OE cells compared to control vector cells (Fig. 4C), indicating their enhanced translation when FXR1 is amplified. mRNAs that are up-regulated in FXR1 overexpression translatome that overlap with increase in AraC-treated proteome are enriched for GC-rich 5′UTRs (fig. S4, A and B) (*1*, *54*, *55*). Several genes known to be translated by non-AUG start sites (*48*) are included among the up-regulated translatome in FXR1 overexpression cells and have GC-rich 5′UTRs (fig. S4, C and D). These GC-rich 5′UTRs and noncanonical start sites are not preferred for conventional tRNA recruitment by eIF2 in the canonical translation mechanism. Therefore, translation of these mRNAs could be enabled by unconventional translation conditions in G0, AraC-treated, and FXR1-overexpressing cells where eIF2α is phosphorylated to reduce its activity. In accord, we find that these unconventional target genes, including those regulated by upstream open reading frames [uORFs; activating transcription factor 4 (ATF4)] (*56*), and noncanonical start sites (CITED1) (*48*) are increased in FXR1 OE but decreased in FXR1 KD cells (fig. S4, E and F), consistent with their need for eIF2α phosphorylation to reduce conventional translation. To test whether these 5′UTRs contribute to specific translation in G0 cells, we constructed a reporter with the 5′UTR of BCL6, one of the translated genes in FXR1 overexpression cells (table S4A) that is also enhanced in G0 and AraC-treated cells (table S3A). We find that the translation efficiency of BCL6 5′UTR luciferase over a control 5′UTR [CX (*10*)] reporter (normalized for Renilla co-transfection control and RNA levels) is elevated in G0 compared to proliferating cells and in FXR1 OE compared to control vector cells (Fig. 4D and fig. S4G). These data suggest that specific mRNA translation involve, in part, distinct 5′UTRs that are enabled upon eIF2α phosphorylation, elicited by FXR1-mediated ribosome changes.

### Impact on translation mechanism

To understand the mechanism of translation, we analyzed polysomes in FXR1-depleted cells compared to control shRNA cells. As in the case of FXR1 OE cells compared to control vector cells (Fig. 4A), while specific genes are altered on polysomes upon FXR1 depletion (table S3, F to H), no significant difference was observed in polysome profiles and in the polysome to monosome (P/M) ratio in profiles conducted in FXR1-depleted cells compared to control shRNA cells (Fig. 4E).

The P stalk proteins are at the guanosine triphosphatase (GTPase) activation center (GAC) near the A site, where eEF1A mediates translation elongation; increased binding of GCN2 in this region via RPLP0 enables GCN2 activation, which is prevented if eEF1A binds GCN2. Thus, GCN2 activation may suggest reduced eEF1A activity and elongation as seen in starvation stress conditions (*39*, *40*, *57*–*59*). Altered elongation has been observed with the FXR1 paralogue, FMRP (*60*). Therefore, as our data showed that GCN2 associates with ribosomes in FXR1 OE cells, but not in control vector cells (Fig. 3K), and is activated because of RPLP0 that increases in FXR1 OE cells (Fig. 3, B and M), we tested whether elongation may be altered in FXR1 OE and KD cells, compared to control cells.

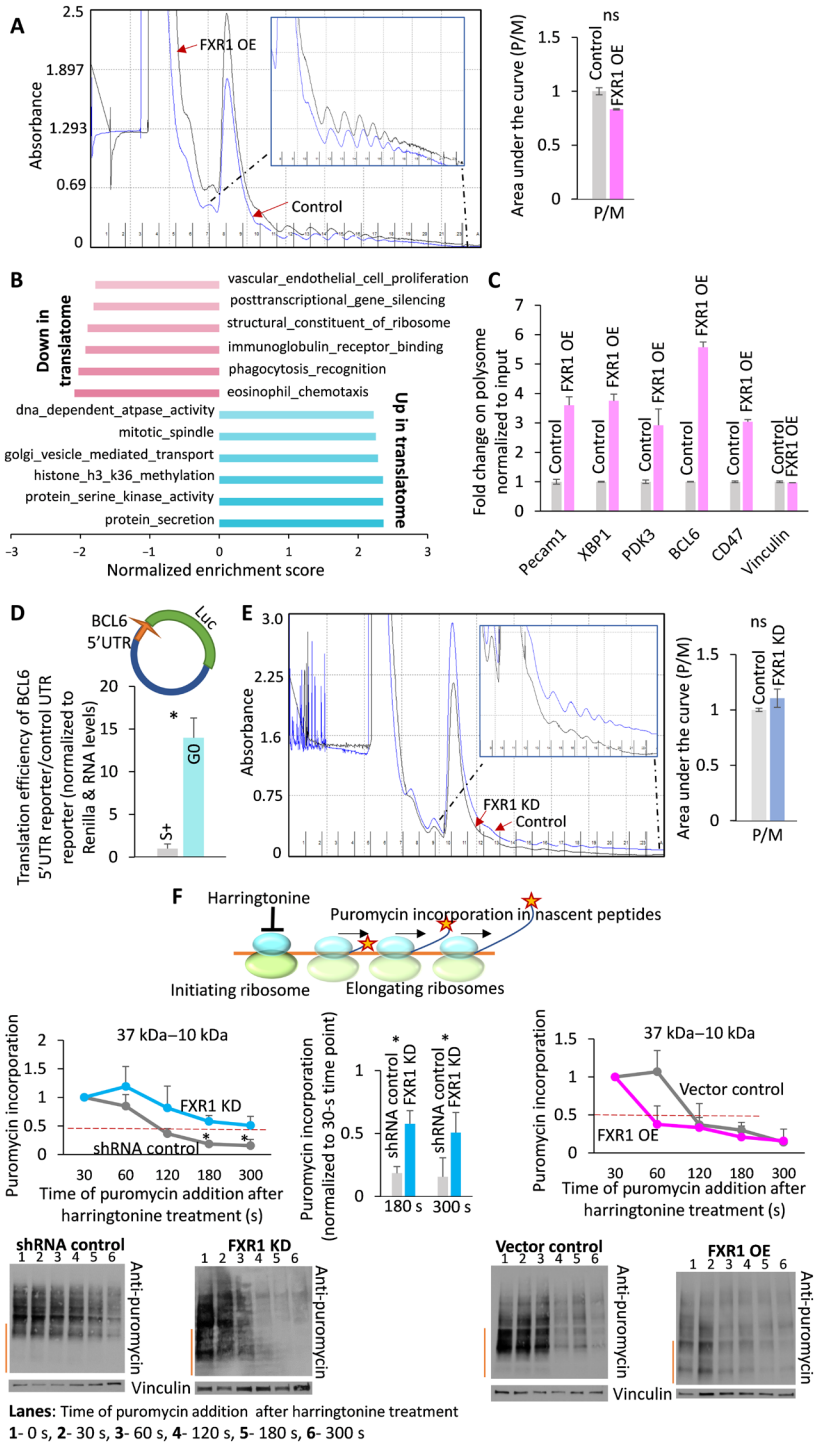


**Fig. 4. FXR1 overexpression promotes translation of prosurvival genes with distinct 5′UTRs.** (**A**) Polysome analysis in FXR1 OE cells compared to control cells. Polysome/monosome (P/M) ratio graphed from three replicates. Global analysis of translatome in FXR1 OE compared to control vector cells. (**B**) Graph showing gene ontology (GO) terms with highest and lowest normalized enrichment score (NES), based on GSEA of FXR1 OE translatome compared to control vector translatome (table S4, A to E). (**C**) qPCR analysis of polysome enrichment of selected mRNAs from FXR1 OE translatome compared to control vector translatome in table S4 (A to C), normalized to inputs. (**D**) Translation efficiency of luciferase reporter bearing BCL6 GC-rich 5′UTR normalized to cotransfection Renilla control reporter and for reporter RNA levels over control 5′UTR CX reporter (*10*) normalized to cotransfection Renilla control reporter and for reporter RNA levels, in G0 compared to serum-grown S+ cells. (**E**) Polysome analysis of FXR1 KD compared to control shRNA cells. P/M ratio graphed from three replicates. (**F**) Harringtonine initiation inhibition assay to assess translation (*61*) by existing elongating ribosomes over time by puromycin labeling, followed by Western analysis (below) for puromycin-labeled proteins and loading control vinculin. Top, graphs of 37- to 10-kDa proteins (orange line) over time in FXR1 KD versus control shRNA cells, of final time points in FXR1 KD versus control shRNA cells, and in FXR1 OE compared to control vector cells. Data are average of three replicates ± SEM. See also fig. S4 and table S4.

We treated cells with harringtonine to block initiation followed by a time course to observe translated products from preexisting elongating ribosomes, with puromycin termination and labeling (SunRiSE method) (*61*). We observed a difference in labeling at the earliest time points (fig. S4H), similar to the nascent global translation in Fig. 1F, suggesting increased translation with FXR1 OE compared to control vector cells that is then blocked by harringtonine. We examined labeled products that were smaller in size, as these would reveal differences in elongation rates first (*61*) (also all proteins). The harringtonine time course shows moderately enhanced labeling with FXR1 KD compared to control shRNA cells (Fig. 4F). FXR1 OE showed a slight, but not significant, trend of decreased labeling, compared to control vector cells. While additional studies are needed, these data hint that FXR1 depletion may moderately increase translation elongation. This is in addition to FXR1's role in increasing translation initiation of specific 5′UTR-bearing mRNAs (Fig. 3, N and O, and fig. S3J, GUG reporter; Fig. 4D and fig. S4G, BCL6 5′UTR reporter), rewiring translation for surviving these conditions.

### FXR1-overexpressing cells show decreased monocyte migration and enhanced survival with macrophages

Our data show altered translation of immune regulators in FXR1-overexpressing cells. On the basis of our data, these cells may subvert immune cells by decreasing translation of immune susceptibility genes (receptors, immune cell–attracting chemokines) while also promoting translation of immune evasion genes (CD47) that inhibit antitumor macrophages (*50*) (Fig. 4B, up and down in translatome genes, and table S4, D and E).

Since FXR1-overexpressing cells show decreased translation of immune-attracting chemokines (Fig. 4B, down in translatome genes, and table S4E), we first tested whether FXR1 overexpression alters migration of monocytes. We find that cocultured monocytes, in a transwell assay, show 50% reduction in monocyte migration toward FXR1 OE cells compared to control vector cells (Fig. 5A and fig. S5A). This is consistent with our data that show decreased translation of immune-attracting chemokines in FXR1-overexpressing cells (Fig. 4B, down in translatome genes, and table S4E) and our data that showed altered immune regulators in G0 and AraC-treated cells (*1*). These data suggest that monocytes are precluded from the environment around FXR1-overexpressing cells through decreased translation of immune-attracting chemokines, which could allow FXR1-overexpressing cells to evade associated antitumor immune activity.

Second, we find that immune evasion genes, elevated in the FXR1 overexpression translatome (table S4, A to D), are also increased in G0 and AraC-treated cells (table S3A) (*1*) and include SLAMF6 (*62*) and CD47 (*50*) that block antitumor immune activity (*50*). Therefore, we tested whether FXR1 OE cells would show increased survival when cocultured with macrophages that can be evaded by CD47, compared to control vector cells. Flow cytometry analysis revealed greater survival of FXR1 OE cells (by 22%) compared to control vector cells, after coculturing with macrophages (Fig. 5B and fig. S5B). These data suggest that FXR1-overexpressing cells translate immune evasion regulators to survive antitumor immunity.

### Chemosurvival of FXR1-overexpressing cells is reduced by drugs that override eIF2α phosphorylation or block translated survival genes, BCL6 and XBP1

The enhanced eIF2α phosphorylation in G0, AraC-treated, and FXR1 OE cells (Fig. 3J and fig. S3H) is a potential vulnerability as these cells use reduced canonical translation to permit specific, prosurvival mRNA translation. To test whether the elevated eIF2α phosphorylation and specific mRNA translation is needed for chemosurvival, we used the small molecule, ISRIB. ISRIB overrides eIF2α phosphorylation and restores canonical translation, which would suppress unconventional, specific mRNA translation (*4*, *63*). We first tested whether the translation observed with FXR1 overexpression can be reversed by ISRIB. Western blot analysis revealed decrease of known noncanonical targets such as ATF4 that are not translated in the presence of ISRIB (fig. S5C). As shown in Fig. 5 (C to E), we performed polysome analysis in FXR1 overexpression cells with or without ISRIB treatment followed by qPCR of mRNAs that are translationally increased in FXR1-overexpressing cells (from table S4A). We find that ISRIB reduced polysome association of several mRNAs that are up-regulated in FXR1-overexpressing cells, without affecting other genes like vinculin (Fig. 5E). These data suggest that FXR1 overexpression promotes specific, prosurvival mRNA translation under eIF2α phosphorylation conditions. If so, then overriding this unconventional translation should reduce chemosurvival of FXR1-overexpressing cells. Consistently, we find that FXR1 OE cells that are treated with ISRIB and AraC have reduced chemosurvival compared to FXR1 OE cells that are treated with buffer and AraC (Fig. 5F). To confirm that the translated genes are important for survival in FXR1-overexpressing cells, chemosurvival was tested after inhibiting two known survival genes (XBP1 and BCL6) that are up-regulated in FXR1-overexpressing cells, compared to untreated, control vector cells (table S4, A to D). We find that treatment of FXR1-overexpressing cells with AraC and toyocamycin, an inhibitor of XBP1 prosurvival gene (*64*, *65*) (Fig. 5G, together, or adding toyocamycin post-AraC treatment), or AraC and FX-1, an inhibitor of BCL6 prosurvival oncoprotein (*49*) (Fig. 5H, adding FX-1 post-AraC treatment), reduced chemosurvival compared to treatment with buffer and AraC and to control vector cells. These data suggest that specific mRNA translation mediated by FXR1 contributes to chemosurvival (Fig. 5I) and is a vulnerability that can be targeted in FXR1 elevated conditions.

## DISCUSSION

Cancer cells can enter a reversible arrest phase called quiescence or G0 that is resistant to harsh conditions including chemotherapy (*1*, *2*). G0 cells induced by serum starvation are chemoresistant-like chemotherapy-surviving leukemic cells and exhibit similar gene expression at the posttranscriptional level (*1*). These data suggest that there is translation of a specific set of survival genes, along with suppression of genes that are detrimental upon therapy treatment. How cells translate specific genes in these clinically relevant conditions is not known and could involve translation mechanism changes. We find that ribosome-associated regulators are similarly altered in both G0 and chemosurviving cells (*1*) (Fig. 1, A and B), indicating that they may mediate this gene expression via mechanistic changes.

FXR1 is an RNA-binding protein that was found associated with ribosomes (*7*) and is a posttranscriptional regulator (*10*) that is amplified at its chromosome locus in several aggressive cancers, where it induces dysregulation of critical gene expression (*9*). Our data revealed that FXR1a isoform is elevated in G0 AML cells (*10*). Since G0 cells are chemoresistant (*1*), this suggests that FXR1 that is increased in G0 could play a role in chemosurvival. In accord, we find that similar to G0 THP1 cells, AraC chemotherapy-treated THP1 and other AML cells (NOMO1) transiently up-regulate FXR1 (Fig. 1C and fig. S1,

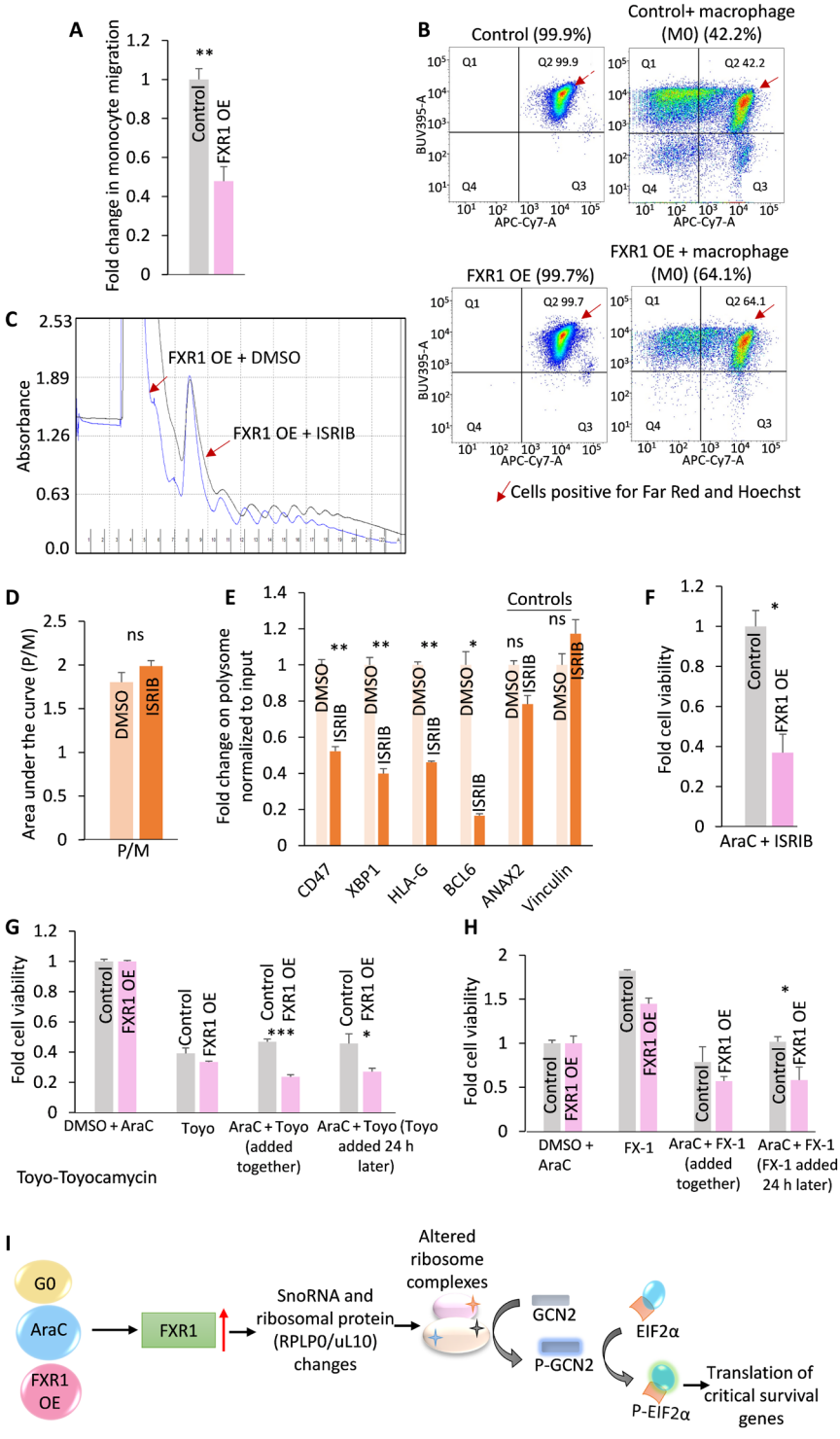


**Fig. 5. Chemosurvival in G0 and AraC-treated cells, and upon FXR1 overexpression, can be reduced by overriding eIF2α phosphorylation, and thereby decreasing translation of survival genes, or by targeting the translated survival genes.** (**A**) Graph of fold change in monocyte migration (image in fig. S5A, stained with Far Red CellTrace dye) in a transwell assay, with FXR1 OE cells or control vector cells in the bottom chamber. (**B**) Flow cytometry data showing survival of control vector cells compared to FXR1 OE cells (stained with Far Red CellTrace dye and Hoechst 33342 to detect live cells in quadrant 2 marked by an arrow) after coculturing with macrophages. (**C**) Polysome analysis of FXR1 OE cells, with or without ISRIB treatment for 24 hours, (**D**) P/M ratio, and (**E**) qPCR analysis for enrichment of FXR1 OE target and control mRNAs (from table S4) on polysomes of ISRIB-treated or untreated FXR1 OE cells, normalized to Input. (**F**) Chemosurvival of FXR1 OE compared to control vector cells, treated with AraC and ISRIB (cotreatment, restores canonical translation, suppressing specific mRNA translation), (**G**) with toyocamycin, XBP1 inhibitor (cotreatment with AraC and post-AraC treatment), and (**H**) with FX-1, BCL6 inhibitor (post-AraC treatment) in FXR1 OE compared to control vector cells, and to FXR1 OE and control vector cells treated with AraC and buffer. (**I**) Model for FXR1-mediated ribosome alterations that induce translation changes to promote AML survival. Data are average of three replicates ± SEM. See also fig. S5 and table S4.

A and B). These data suggest that FXR1 could be increased in some cancers treated with therapies like AraC to promote chemosurvival. Consistently, we find that overexpression of FXR1a that is elevated in G0 (*10*) promotes AraC survival by almost twofold, while knockdown of FXR1 reduces chemosurvival to less than 50% (Fig. 1, D and E). These data suggest that FXR1 mediates chemosurvival in G0 and chemo-treated AML, where it is elevated.

FXR1 was identified associated with the ribosome (*7*), and we previously found that FXR1 associates with and promotes translation of specific mRNAs in G0 (*10*). Therefore, the role of FXR1 in chemosurvival could involve translation regulation. To test this, we analyzed translation in cells with or without FXR1 depletion by nascent translation labeling. We find that in FXR1-depleted cells, translation is decreased by almost half, compared to control shRNA cells (Fig. 1F and fig. S1C), while increased by 1.7-fold in FXR1-overexpressing cells. These data suggest a role for FXR1 in G0 and chemo-treated cells via translation regulation that may promote chemosurvival observed here.

FXR1 is known to be nucleolar, nuclear, and cytoplasmic (*8*) and can participate in ribosome biogenesis at multiple levels: through known associations with ribosomes and RPs (*7*), with RNA regulators, and by posttranscriptional control over ribosome regulators as detected previously (*10*, *35*). We find that FXR1 depletion reduces all rRNAs and decreases several snoRNAs and RPs that increase in G0; conversely, FXR1a overexpression leads to their increase (Fig. 2, A to C; fig. S2A; and table S1). FXR1 regulates levels of snoRNAs (table S1, A to C) that modify rRNA sites that affect translation (*25*–*29*). In accord with the increase of snoRD58A and snoRA22 upon FXR1 elevation in AraC-treated cells and FXR1-overexpressing cells, we find increased modification at their rRNA target sites on 28*S* rRNA (Fig. 2, D and E). In addition, with multiple snoRNA changes, alterations in other rRNA modifications are observed by mass spectrometry upon FXR1 depletion (Fig. 2F, fig. S2B, and table S1D). FXR1 depletion and overexpression also alters U3 and U8 snoRNAs (Fig. 2B and fig. S2A) that cleave and process 47*S* Pol I precursor rRNA (*16*, *19*–*22*), which would lead to the observed alteration in mature 28*S*, 18*S*, and 5.8*S* rRNA levels (Fig. 2A and fig. S2A). These data suggest that FXR1 affects multiple ribosomal components (table S1, Fig. 2, and fig. S2), which could cause the translation change observed in AraC-treated and G0 cells (Fig. 1F and fig. S1C) where FXR1 is amplified (Fig. 1, A to C, and fig. S1, A and B).

To understand how FXR1 enables these ribosome changes, we analyzed the FXR1 protein interactome (table S2). We find that FXR1 associates with snoRNA and ribosome biogenesis regulators, such as NOLC1 (*30*, *31*) (Fig. 2G), other ribosome-associated factors (table S2 and fig. S2C), and rRNAs (fig. S2D). Consistent with the fact that both Pol I–transcribed rRNAs and Pol II–transcribed snoRNAs and RPs are affected by FXR1, we find that FXR1 interacts with DDX21 (Fig. 2H), a regulator that promotes Pol I and Pol II ribosome gene transcription (*32*, *33*). In accord, we find that DDX21 overexpression, but not of a control vector, partially rescues the reduced 45*S* rRNA precursor levels in FXR1 knockdown cells (Fig. 2I). This is consistent with regulation of ribosomes, as DDX21 also binds snoRNAs including U3 to promote their levels and functions and enhances Pol I– and Pol II–derived ribosome gene transcription (*32*–*34*). Given that all four rRNAs are affected by FXR1, including 18*S*, 28*S*, and 5.8*S* rRNAs from Pol I transcription, and Pol III transcript, 5*S* rRNA, our data suggested that FXR1 may influence a common rRNA transcription factor for Pol I and Pol III, and/or for all three RNA polymerases, as FXR1 also affects Pol II–derived RPs and snoRNAs. Consistent with recent data showing FXR1 regulation of c-MYC (*35*) that controls ribosome gene transcription from all three polymerases (*36*), we find that c-MYC increases with FXR1 overexpression (Fig. 2J). In addition, we find that FXR1 associates with the mRNA of POLR1D, a Pol I and Pol III transcription factor; consistently, FXR1 depletion decreases, while overexpression increases, POLR1D (Fig. 2, K and M, and fig. S2E). As POLR1D is needed for rRNA transcription from Pol I and Pol III, and for DDX21 localization and thus DDX21-controlled snoRNAs and Pol I and Pol II ribosome biogenesis (*32*, *34*), FXR1 regulation of POLR1D would affect all four rRNAs (Fig. 2A). The levels of mature rRNAs and the precursor 45*S* are differentially affected. This may be due to additional effects, apart from transcription and processing regulation by MYC, DDX21, and PolR1D, where rRNA levels and folding, and thereby stability, may be affected by altered modifications by snoRNAs and RPs, whose levels are regulated by FXR1. Thus, our data reveal that FXR1 modulates multiple ribosome regulators, which can lead to ribosome changes upon FXR1 elevation in G0 chemoresistant cells.

These data suggest multiple changes in the ribosome, upon FXR1 overexpression that is seen in G0 and AraC-treated cells (Figs. 2 and 3, A to D; fig. S3A; and tables S1 and S3). Consistently, we find that ribosomes migrate differently in two distinct complexes in G0 and AraC-chemoresistant cells compared to one in proliferating cells; this is also observed with FXR1 overexpression compared to control vector (Fig. 3, E and F, and fig. S3, B to E), indicating that FXR1 induces similar differences in ribosome complexes. As these complexes in cytoplasmic extracts are associated with Y10B that binds 5.8*S* in 80*S* (*38*), they may include partially processed 80*S* complexes in the cytoplasm where 18*S* is still being processed, causing differences in 18*S* and 28*S* rRNA levels observed. These ribosome changes can alter translation, which could enable the cells to adapt to chemotherapy and survive.

One way that ribosome changes could alter translation would be by activating stress signaling. Ribosomes not only function as translation machineries but also can directly activate stress signaling pathways (*39*–*42*). This includes GCN2 that is activated by stalled ribosomes (*57*) or by P stalk RPs (*39*, *40*), and PKR that can be activated by snoRNAs (*43*, *44*). These kinases disable canonical translation via eIF2α phosphorylation, which permits translation on specific mRNAs such as those with noncanonical start sites or complex 5′UTRs (*3*, *46*–*48*). In accord, we find that FXR1 overexpression leads to activation of PKR and GCN2 (Fig. 3, G and I). Overexpression of FXR1 can increase specific snoRNAs that can bind and activate PKR, a dsRNA binding protein (*43*, *44*), which can cause eIF2α phosphorylation. Consistently, we find that overexpression of G0 up-regulated snoRNAs, snoRD46, or snoRA2A leads to increased eIF2α phosphorylation (Fig. 3H and fig. S3F). In accord, previous data had shown that overexpression of fibrillarin that leads to altered snoRNA-mediated rRNA modification induces noncanonical translation (*24*). We find that RPs including P stalk RPs are altered in FXR1 OE and KD cells and in G0 and AraC-treated cells (Fig. 3, B and C; fig. S3A; and table S3, B, C, E, and G). Changes in the P stalk RPs can lead to GCN2 activation and eIF2α phosphorylation via GCN2 interaction with RPLP0 (*39*, *40*). Consistently, we find that FXR1 overexpression enhances RPLP0 that is also seen in AraC-treated cells, and leads to GCN2 phosphorylation and eIF2α phosphorylation (Fig. 3, I and J). RPLP0 associates with GCN2; consistently, in FXR1 overexpression cells where RPLP0 is elevated along with eIF2α phosphorylation, we find

increased association of GCN2 with ribosomes and RPLP0 (Fig. 3K). In accord, in FXR1-depleted cells, we find that eIF2α phosphorylation is decreased (Fig. 3L and fig. S3G). Accordingly, RPLP0 depletion in FXR1-overexpressing cells attenuated phosphorylation of GCN2 and eIF2α (Fig. 3M), indicating that RPLP0 is needed for eIF2α phosphorylation, elicited in FXR1 overexpression conditions. This increase in FXR1 and eIF2α phosphorylation is regulated over time of AraC treatment and is variable at high AraC concentrations (fig. S3, H and I), likely due to multiple effects including cell death and feedback regulation of phosphatases and mTOR that are shown to affect eIF2α phosphorylation and FXR1 levels (*1*, *10*, *45*). Together, these data suggest that increased FXR1 in G0 chemosurviving cells alters ribosomes to induce stress signals that inhibit canonical translation and permit specific mRNA translation.

Such stress signaling by the ribosome has been observed with colliding ribosomes that trigger GCN2-mediated eIF2α phosphorylation that leads to survival or, at increased levels, induce stress c-Jun N-terminal kinase (JNK)/p38 mitogen-activated protein kinase (MAPK) signaling pathway to trigger apoptosis. This has also been observed with c-GAS signaling in other conditions, as well as with ribotoxic agents, leading to gene expression changes (*41*, *42*, *66*, *67*). With transient, acute ISR, there is global decrease in translation followed by restoration, but with chronic, moderate ISR, such as seen in some stress conditions, there is distinct gene translation (*68*, *69*). This can result in reprogramming of translation without drastic reduction in overall translation as seen in FXR1 OE cells where translation increases (Fig. 1F), despite eIF2α phosphorylation (Fig. 3, I to M, and fig. S3, H and I). How this is elicited, whether this is due to MYC deregulation (*35*) and of other ribosome regulators (Fig. 2, G to M) and stress mechanisms by FXR1 in these conditions, needs to be further investigated. With eIF2α phosphorylation, stringent use of conventional Kozak start sites for initiator tRNA recruitment (*3*) is reduced—and can permit translation of specific mRNAs such as those with complex 5′UTRs, unconventional non-AUG start sites, or AUGs in poor Kozak start sites that would normally be poorly translated (*47*). In accord, we find that translation of a reporter with a noncanonical GUG start site over that of a reporter with a conventional AUG start site is promoted in FXR1-overexpressing cells and in G0 and chemo-treated cells, compared to untreated serum-grown proliferating control vector cells (Fig. 3, N and O, and fig. S3J). Consistently, global profiling revealed that many of the genes up-regulated in G0, AraC-treated, and FXR1-overexpressing cells (Fig. 4, A to C, and table S4) have GC-rich 5′UTRs (fig. S4, A to D), and non-AUG start sites (*48*), and include noncanonical translation targets (table S4 and fig. S4, C to F); these genes may need eIF2α phosphorylation to be translationally up-regulated. In accord, we find that a reporter bearing the GC-rich 5′UTR of one of these up-regulated genes, BCL6, shows enhanced translation over a control 5′UTR reporter, in G0 and FXR1 overexpression cells, compared to serum-grown, control vector cells (Fig. 4D and fig. S4G), independent of RNA levels. Other features that are unique to these transcripts such as previously identified 3′UTR elements (*1*, *10*), and other ribosomal and translational changes, may also contribute to the specific translation observed.

Our findings of multiple effects of FXR1 on the ribosome (Figs. 1 and 3) reveal the complexity of translation changes in these chemoresistant AML cells where FXR1 is amplified. Analysis of P/M ratios did not reveal differences between FXR1 OE and FXR1 KD compared to control cells (Fig. 4, A and E). The P stalk RPLP0/uL10 is at the GAC near the A site, where eEF1A mediates translation elongation; increased binding of GCN2 in this region via RPLP0 enables GCN2 activation, which is prevented if eEF1A binds GCN2. Thus, GCN2 activation may suggest reduced eEF1A activity and elongation as seen in starvation stress conditions (*39*, *40*, *57*–*59*). To test this, we did a harringtonine initiation block experiment to block initiation and see preinitiated, elongating ribosome runoff with puromycin labeling (*61*). We observe more labeling over time in FXR1 KD compared to control cells (Fig. 4F and fig. S4H). These data hint that runoff production from elongating ribosomes after initiation shutdown with harringtonine may be moderately enhanced in FXR1 KD compared to control cells. This was first observed with the paralogue of FXR1, FMRP, that not only suppresses translation elongation of specific targets but also promotes initiation of other distinct mRNAs (*60*, *70*). While additional studies are needed, these data suggest that FXR1 rewires translation—by increasing initiation of specific 5′UTR-bearing or noncanonical start site–bearing mRNAs (Fig. 3, N and O, and fig. S3J, GUG reporter; fig. S4G and Fig. 4D, BCL6 5′UTR reporter) that are likely needed for survival—and may also possibly affect elongation slightly (Fig. 4F), potentially of mRNAs that were being translated in untreated cells and need not be translated upon therapy or G0 conditions.

Our data reveal that prosurvival genes—stress response genes like XBP1 (*64*, *65*), cell adhesion genes like PECAM1 (*52*), immune genes like CD47 (*50*), and oncoproteins like BCL6 (*49*) (table S4, A to D, and Fig. 4B)—are translated via these ribosome changes that are triggered by FXR1 in G0 chemosurviving cells. Genes that are down-regulated in the FXR1 overexpression translatome compared to control vector cells include immune susceptibility genes (receptors, immune-attracting chemokines, Fig. 4B, down in translatome genes, table S4E). Consistently, we find that monocyte migration is reduced by 50% in transwell assays with FXR1-overexpressing cells compared to control vector cells (Fig. 5A and fig. S5A), which could allow FXR1-overexpressing cells to evade antitumor immune activity. Concurrently, the increased translatome in FXR1-overexpressing cells include antitumor immune evasion genes such as CD47 (Fig. 4, B and C, and table S4, A to D) that inactivate antitumor macrophages (*50*). In accord, we find that FXR1-overexpressing cells show increased survival compared to control vector cells when cocultured with macrophages (Fig. 5B and fig. S5B). Together, these data suggest that the specific translatome elicited in FXR1-amplified conditions, as in G0 and AraC-treated cells, subverts antitumor immunity by decreasing immune susceptibility genes and by translating antitumor, immune evasion genes to survive antitumor immune activity.

Inhibition of canonical translation by eIF2α phosphorylation can lead to expression of specific survival mRNAs that are poorly translated by the canonical mechanism (*1*, *47*, *55*) due to unconventional start sites or GC-rich 5′UTRs (fig. S4, A to D). Consistently, treatment with ISRIB that overrides eIF2α phosphorylation to restore canonical translation (*4*, *63*) prevents this specific mRNA translation (Fig. 5, C to E, and fig. S5C). Thus, these data suggest that FXR1 increase in G0 and AraC-treated cells causes ribosomal changes that can reduce canonical translation and enable translation of specific genes by triggering eIF2α phosphorylation.

Together, our data suggest that the enhanced chemosurvival in FXR1-overexpressing cells—as in G0 and AraC-treated cells, where FXR1 is elevated and causes ribosome changes and eIF2α phosphorylation—could be reversed by targeting the eIF2α phosphorylation–induced, specialized translation mechanism, or such translated genes. Consistently, we find that inhibition of this specific mRNA translation

with ISRIB (Fig. 5F), or inhibition of the downstream target genes such as that of XBP1 (*64*, *65*) or of BCL6 (*49*) with pharmacological inhibitors (Fig. 5, G and H), reduces the chemosurvival of FXR1 overexpression cells, compared to control vector cells or to FXR1 overexpression cells treated with chemotherapy alone. Together, our data reveal that FXR1 is a critical translation regulator that is amplified in G0 and chemosurviving AML, which induces ribosome changes that trigger stress signals to enable specialized translation of survival genes to promote tumor persistence (Fig. 5I).

### Limitations

While we verified our findings in two different AML backgrounds, further studies in vivo are needed. Given the complexity of ribosomal changes observed (Figs. 1 to 4 and figs. S1 to S4), apart from the eIF2α phosphorylation mechanism, the impact on G0 and chemosurviving AML will include effects of other ribosome changes mediated by FXR1, other gene expression regulation by FXR1, and other dysregulated RNA mechanisms in G0 cells (*1*) to elicit survival of G0 and chemoresistant AML.

## MATERIALS AND METHODS

### Cell culture

THP1 cells were cultured in RPMI 1640 medium supplemented with 10% fetal bovine serum (FBS), 2 mM L-glutamine, streptomycin (100 μg/ml), and penicillin (100 U/ml) at 37°C in 5% $CO_2$. SS or G0 THP1 cells were prepared by washing with phosphate-buffered saline (PBS) followed by serum starvation at a density of $2 \times 10^5$ cells/ml. AraC-treated cells were prepared by treatment with indicated concentrations of AraC for indicated periods of time. THP1 (TIB-202) and monocytes (CRL9855) were obtained from the American Type Culture Collection (ATCC). NOMO1 and MOLM13 were obtained from ATCC and from the Scadden group (*1*). Cell lines were tested for mycoplasma (Promega) and authenticated by the ATCC Cell Authentication Testing Service (*1*).

### Plasmids

TRIPZ and GIPZ plasmids expressing shRNAs against human FXR1, RPLP0, and control vector expressing miR30a primiR sequences (RHS4750) were obtained from Open Biosystems–Dharmacon (shRNA target sequences are in table S5). Stable cell lines were constructed as described previously (*10*, *11*). The stable cells expressing shRNA against FXR1 were induced with doxycycline (1 μg/ml) for 3 days (once each day) to knock down FXR1. Control cells were treated similarly. THP1 FXR1 OE cell lines were created by transducing cells with pHAGE retroviral vector containing FXR1a for constitutive overexpression of FXR1a (*10*, *11*). Renilla was obtained and used as done previously (*10*). The 5′UTR of BCL6 mRNA was amplified (with primers flanked by Nhe I restriction sites). CX plasmid (*10*) and BCL6 5′UTR-containing amplicon were digested with Nhe I [New England Biolabs (NEB)] followed by ligation with T4 DNA ligase (NEB). Ligation mixes were transformed in *Escherichia coli* cells. Plasmids were purified from *E. coli* cells after transformation. Positive clones were confirmed by sequencing. DDX21 plasmid (*71*) and GUG and AUG luciferase reporters (*72*) were obtained from Addgene (p23-DDX21 WT was a gift from L.-L. Chen, Addgene plasmid #128803; pGL4.13/AUG-FFLuc-3XFLAG and pGL4.13/GUG-FFLuc-3XFLAG were gifts from J. Wilusz, Addgene plasmids #127333 and #127334).

### Polysome profiling and microarray

Cells ($30 \times 10^6$) were grown for each sample and harvested on ice. In case of the FXR1 KD and its respective control, and FXR1 OE and its respective control, treated with ISRIB or dimethyl sulfoxide (DMSO), cycloheximide was not used. Sucrose was dissolved in polysome buffer containing 100 mM KCl, 5 mM $MgCl_2$, 2 mM dithiothreitol (DTT), and 10 mM tris-HCl (pH 7.4). Sucrose gradients from 10 to 55% were prepared in ultracentrifuge tubes (Beckman) as previously described (*1*). Harvested cells were rinsed with ice-cold PBS and resuspended in polysome buffer with 1% Triton X-100 and murine ribonuclease (RNase) inhibitor (40 U/ml; NEB) for 20 min with intermittent tapping on ice for lysis. After centrifugation of cell lysates at 10,000 rpm for 10 min, supernatants were loaded onto sucrose gradients followed by ultracentrifugation (Beckman Coulter Optima L90) at 32,500 rpm at 4°C for 80 min in the SW40 rotor. Samples were separated by density gradient fractionation system (Biocomp Piston Gradient Fractionation). RNAs were purified from heavy polysome fractions and whole-cell lysates. The synthesized complementary DNA (cDNA) probes from the WT Expression Kit (Ambion) were hybridized to Gene Chip Human Transcriptome Array 2.0 (Affymetrix) and analyzed by the Partners Healthcare Center for Personalized Genetic Medicine Microarray and BUMC facilities. Gene ontology (GO) analysis for differentially expressed translatome or proteome was conducted by DAVID 6.7 tools (*73*). Molecular signatures enriched in FXR1 OE, KD, and control cells were identified by gene set enrichment analysis (GSEA) (*74*).

### Western blot analysis

Cells were collected and resuspended in lysis buffer containing 40 mM tris-HCl (pH 7.4), 6 mM $MgCl_2$, 150 mM NaCl, 0.1% NP-40, 1 mM DTT, 17.5 mM ß-glycerophosphate, 5 mM NaF, and protease inhibitors. Cell lysates were heated at 95°C with 200 mM DTT and 1× SDS loading dye for 10 min. Samples were loaded onto 4 to 20% gradient SDS-PAGE (Bio-Rad) or 16% SDS-PAGE (Invitrogen), transferred to nitrocellulose membranes, and processed for immunoblotting. Antibodies against FXR1 (05-1529) (used for Western), actin (MAB1501), and tubulin (05-829) were from Millipore; NOLC1 (11815-1-AP), DDX21 (10528-1-AP), PolR1D (12254-1-AP), RPLP0 (11290-2-AP), RPLP2 (16805-1AP), RPL29 (15799-1-AP), RPL19 (14701-1-AP), vinculin (26520-1-AP), ATF4 (10835-1-AP), GADD34 (10449-1-AP), and FXR1 (13194-1-AP) (used for Immunoprecipitation) were from ProteinTech; PKR (3072S), P-PKR (2611S), EIF2α (9722S), P-EIF2α (3597S), and GCN2 (3302S) (used for immunoprecipitation) were from Cell Signaling Technology; c-Myc (ab32072), P-GCN2 (ab75836), GCN2 (ab134053), and ATF4 (ab23760) (used for Western blot) were from Abcam; and anti-puromycin [3RH11] (EQ0001) was from Kerafast.

### Mass spectrometry

Multiplex quantitative proteomics analysis (TMT spectrometry) was conducted, as done previously (*10*), from THP1 leukemic cells and cell lines created that were treated as described.

### Quantitative RT-PCR

Total RNA was extracted using proteinase K buffer and TRIzol (Invitrogen) as performed previously (*10*). The cDNA was synthesized from 1 μg of RNA using M-MuLV Reverse Transcriptase (NEB) and random hexamer primer (Promega). qPCRs were run on LightCycler

480 Instrument II (Roche) using 2× SYBR green mix (Bio-Rad). All primers used are listed in table S5.

### ddPCR assay

ddPCR was performed using purified cDNA obtained from reverse transcription of RNA isolated from cell lines. The assay development for ddPCR validation of target genes of interest was performed in compliance with the updated 2020 Minimum Information for Publication of Digital PCR Experiments (dMIQE) Guidelines. The ddPCR was performed in the Applied Biosystems 96-well Thermal Cycler (Thermo Fisher Scientific) in a final volume of 20 µl. The optimized reaction mixture was prepared using 10 µl of ddPCR EvaGreen Supermix (Bio-Rad), 1000 nM forward and reverse primers, and 1 µl of diluted cDNA. Dilution of cDNA for different assays was performed as follows: FXR1 (4 ng/µl), U3 (0.2 ng/µl), and 28*S* (0.04 ng/µl). The prepared reaction mixture was transferred to the wells of DG8 cartridge. To generate the droplets, 70 µl of droplet generation oil for EvaGreen (Bio-Rad) was added and the plate was loaded into the QX200 droplet generator (Bio-Rad). The droplet emulsions were then carefully transferred to a semi-skirted, PCR-clean 96 well plate (Eppendorf) using a multichannel pipette. Last, the plate was sealed using PX1 PCR plate sealer (Bio-Rad). Annealing temperature for each assay was determined using a temperature gradient as follows: FXR1 (57°C), U3 (55°C), and 28S (55°C). The final thermal cycling conditions were as follows: initial enzyme activation at 95°C (51% ramp) for 5 min, then 40 cycles of denaturation at 94°C (51% ramp) for 30 s, and annealing/extension at optimized temperature for 1 min, followed by enzyme inactivation at 98°C for 10 min and final hold at 4°C until analysis. Droplets were analyzed using a QX 200 droplet reader (Bio-Rad), and data were acquired and analyzed with QuantaSoft analysis software (Bio-Rad). The number of target gene copies per 20 µl of reaction was calculated from QuantaSoft data. Only samples with >10,000 droplets per well were included in the analysis. Three wells are analyzed in parallel for each sample.

### Mass spectrometry for RNA modification analysis

Total RNA was isolated using TRIzol as described previously (*1*, *10*). Isolated RNAs were cleaned using an RNeasy kit (Qiagen). Poly(A)-containing RNAs were separated from the RNA pool using Poly(A) mRNA Isolation System IV (PolyATtract, Promega). The remaining nonpolyadenylated RNA was sent for nucleoside digestion and LC-MS/MS analysis to Arraystar Inc. (www.arraystar.com/lc-ms-based-rna-modification-analysis-service-selected/isolated-rna/).

### Nascent translation level analysis

Global translation was measured by metabolic labeling for a short period followed by PAGE and scintillation analysis. THP1 stable cell lines were grown in normal RPMI medium to prevent additional cellular stress from methionine-free medium. Nascent translation was analyzed using HPG, an amino acid analog of methionine containing an alkyne moiety that can be biotinylated by Click-iT chemistry (Thermo Fisher Scientific). Nascent protein translation labeling with HPG was followed by SDS-PAGE and Western analysis of labeled nascent proteins with HRP-streptavidin antibody. HPG was added as described in the manufacturer's protocol, or alternatively, 100 µCi of $^{35}$S-methionine was added to 10 ml of cells. After incubation at 37°C for 45 min, cells were washed once with PBS and lysed in buffer [40 mM tris-HCl (pH 7.4), 6 mM $MgCl_2$, 150 mM NaCl, 0.1% NP-40, 1 mM DTT, and protease inhibitors]. The lysate was first separated by electrophoresis on an SDS-PAGE gel and then transferred to a nitrocellulose membrane by Western blotting with anti-biotin antibody, or the radiolabeled blot was exposed to a phosphoimager (GE Healthcare). These were quantified by ImageJ. Radiolabeled lysates were also measured by scintillation counter.

### Low dNTP RT-qPCR assay

For analysis of 2'-*O*-methylation, RNA was prepared from indicated cells. Reverse transcription (as described above in qPCR) was performed with primers in the reverse orientation from the modification site on rRNA. Two different dNTP concentrations were used for each primer, low (0.025 mM) and high (2.5 mM). qPCR was done with the resulting cDNA using primers at forward and reverse orientation to the modified sites. Fold change in modification was calculated on the basis of difference of $C_t$ values in the low and high dNTP conditions (*24*). For analyzing pseudouridylation, first, the RNA was treated with CMC metho-*p*-toluene sulfonate [1-cyclohexyl-(2-morpholinoethyl) carbodiimide metho-*p*-toluene sulfonate] under alkaline conditions (*21*, *23*, *24*). This was followed by the process for low dNTP RT-qPCR, as described above for 2'-*O*- methylation. Primers are listed in table S5.

### In vivo crosslinking and immunoprecipitation

In vivo crosslinking using 0.3% formaldehyde and nuclear-cytoplasmic separation were done as described earlier (*1*, *10*). Briefly, around $10 \times 10^6$ to $15 \times 10^6$ cells were harvested on ice followed by washing with cold PBS. Cell pellets were resuspended in hypotonic buffer [10 mM tris (pH 8), 1.5 mM $MgCl_2$, and 10 mM KCl]. A syringe with 25-gauge × $^5/_8$ precision glide needle was used to lyse the cells by repetitive passes through the needle (up to 5 to 10 times to ensure lysis) or, alternatively, a douncer was used to appropriately lyse the cells. The decanted supernatant (cytoplasmic fraction) was centrifuged at 2000 rpm for 10 min at 4°C. The supernatant was again decanted at 2000 rpm for 10 min, producing the final cytoplasmic fraction. The remaining pellet was washed with 10 times the pellet volume with buffer B [20 mM tris-HCl (pH 8.0), 25% glycerol, 1.5 mM MgCl2, 0.2 mM EDTA (pH 8.0), and 20 mM KCl]. After removal of the wash buffer, the pellet was again suspended in a mix of 10 times the pellet volume of buffer B, and five times the pellet volume of buffer C [20 mM tris-HCl (pH 8.0), 25% glycerol, 1.5 mM MgCl2, 0.2 mM EDTA (pH 8.0), and 1.2 M KCl], and the solution was mixed by vortex before a 45-min incubation with nutation at 4°C. If the cells had been crosslinked, this fraction was sonicated for 5 s and then 30-s cooling on ice (six times, 90% duty cycle, output control at 2) and deoxyribonuclease I (Dnase I)–treated before being centrifuged at 2000 rpm for 10 min at 4°C. The decanted supernatant was collected as the nuclear fraction. The supernatant was mixed with the cytoplasmic fraction. Where mentioned, only cytoplasmic fraction was used. The lysates were precleared of nonspecific binders by incubating with protein G (Santa Cruz Biotechnology) beads and IgG. The precleared lysates were incubated with antibodies and IgG (control) overnight in buffer (40 mM Hepes, 100 mM NaCl, 6 mM $MgCl_2$, 0.025% NP-40, 1 mM DTT, 10% glycerol, 1 mM phenylmethylsulfonyl fluoride). Lysates were then incubated with equilibrated and blocked protein G beads for 2 hours. Beads were then pelleted and washed four times with radioimmunoprecipitation assay buffer. Beads were then used to analyze proteins or RNA after using heat to break Schiff's linkages from formaldehyde, followed by proteinase K digestion buffer treatment for the fractions for RNA analysis, and RNase and Micrococcal Nuclease (to remove RNA and DNA) treatment for the fraction for protein analysis as described earlier (*1*, *10*).

### DEAE fractionation assay

DEAE fractionation was performed with in vivo formaldehyde crosslinked extracts or Y10B antibody immunoprecipitates as done previously (*10*). Cell lysates or fractions after Y10B immunoprecipitation were incubated with equilibrated DEAE beads for 2 hours in buffer (40 mM Hepes, 6 mM $MgCl_2$, 2 mM DTT, 10% glycerol, and 150 mM NaCl). After collection of the flow-through, beads were incubated with wash buffer of increasing salt concentrations (40 mM Hepes, 6 mM $MgCl_2$, 2 mM DTT, and 10% glycerol, with NaCl ranging from 250 to 500 to 750 to 1000 to 2000 mM). RNA was isolated from each salt fraction. Amount of rRNA in each fraction was analyzed by qRT-PCR, normalized to input levels.

### Luciferase assay

Plasmids containing firefly luciferase reporters downstream of AUG or GUG start sites (*72*) or the BCL6 5′UTR were co-nucleofected using Lonza Nucleofector (*10*) with Renilla luciferase in FXR1 OE, control vector, and THP1 cells. Nucleofected cells were then grown under conditions of S+, G0, and 5 μM AraC. Cells were harvested, washed, and lysed in 1× passive lysis buffer (Promega). Luciferase activity in the lysates was analyzed using the Luciferase Assay System (Promega) as per the manufacturer's instructions and as conducted previously (*10*).

### Harringtonine initiation block assay

We used harringtonine to block initiation followed by a short time course to observe translated products from preexisting elongating ribosomes, with puromycin termination and labeling [SunRiSE method (*61*)]. Cells were divided into six-well plates and treated with harringtonine (2 μg/ml; Cayman Chemicals, catalog no. 26833-85-2). After indicated time of harringtonine treatment, cells were treated with puromycin (10 μg/ml; Santa Cruz Biotechnology, catalog no. CAS-58-58-2) for 8 min. Cells were pelleted, washed with cold PBS, and lysed in lysis buffer. Lysates were fractionated on a 4 to 20% gradient SDS-PAGE followed by immunoblotting. Anti-puromycin antibody (Kerafast) at a concentration of 1:1000 was used for immunoblotting. ImageJ was used to quantify the whole lane as well as the puromycin labeling of smaller proteins that report differences first (*61*).

### Coculture of leukemic cells with immune cells followed by flow cytometry

CRL9855 monocytes were tested as monocytes or differentiated to M0 macrophages with PMA (phorbol 12-myristate 13-acetate; 185 ng/ml) for 24 hours. M0 macrophages were then treated with interleukin-4 (20 ng/ml) and interleukin-13 (20 ng/ml) for 48 hours for polarization to M2, and with interferon-γ (20 ng/ml) and tumor necrosis factor α (TNFα) (20 ng/ml) for 48 hours for polarization to M1 (*75*). Control and FXR1 OE cells were stained with Far-Red CellTrace dye (Thermo Fisher Scientific) as per the manufacturer's instructions. Macrophages were cocultured with stained control and FXR1 OE cells for 12 hours at a ratio of 1:2. Coculture cells were collected after trypsinization and washed with PBS. Non-cocultured control and FXR1 OE cells, stained with Far Red CellTrace, were used as controls. Harvested cells were thoroughly washed and stained with Hoechst 33342 (Thermo Fisher Scientific) as per the manufacturer's instructions. Samples were filtered through a nylon mesh filter and analyzed for the population stained with both dyes by flow cytometry (*76*). Control cells without the Far Red CellTrace but stained with Hoechst were used as baseline, and the data were analyzed using FlowJo software.

### Cell migration assay

Cell migration assay was performed as previously described (*11*). Transwell chambers (8 μm pore, Corning) were preequilibrated with serum-free medium. CRL9855 monocytes ($2 \times 10^4$ per chamber) that were prestained for 1 hour per the manufacturer's instructions with Far Red CellTrace dye (Thermo Fisher Scientific) were placed in the top chamber, and 700 μl of control or FXR1 overexpression cells was placed in the bottom chamber. The chambers were incubated at 37°C for 18 hours in 5% $CO_2$. Cells on the upper surface of the filter were removed with a cotton swab. Migrated stained monocyte cells were observed in the bottom chamber and visualized using a microscope. Microscope images were taken, and the numbers of migrated cells were determined.

### Inhibitors

Cytarabine (AraC) (*77*), trans-ISRIB (*4*, *63*), FX-1 (*49*), and toyocamycin (*64*, *65*) were obtained from Cayman Chemicals. FXR1 OE and control cells were treated with 1 μM trans-ISRIB for 24 hours. For cell viability that was measured by trypan blue staining and cell counts (*1*), FXR1 OE and control cells were treated individually or with a combination of 5 μM AraC and 1 μM trans-ISRIB for 24 hours, 100 nM toyocamycin and 1 μM AraC, and 10 μM FX-1 and 5 μM AraC.

### Motif, GO, GSEA, and RNAFOLD analysis

Multiple Em for Motif Elicitation (MEME) software was used to search for 5′UTR elements as described earlier (*1*, *78*), using 5' UTR sequences from GenBank. GO analysis for differentially expressed translatome or proteome was conducted by DAVID 6.7 tools (*73*), as described earlier (*1*) with our datasets. GSEA (*74*) was performed as described earlier (*1*) with our datasets. 5′UTR folding as shown in fig. S4 (A and B) was performed using RNAFold web server from the Vienna RNA package (rna.tbi.univie.ac.at/cgi-bin/RNAWebSuite/RNAfold.cgi) (*79*).

### Statistical analyses

Each experiment was repeated at least three times. Sample sizes were estimated on the basis of availability and previous experiments (*10*). No samples were excluded from analyses. Statistical tests were conducted for each figure. SEM values are shown as error bars in all figures. *P* values less than 0.05 were indicated with an asterisk. *E* values were used for the statistical significance in the motif analysis. Statistical analyses for the datasets were performed as described. For the microarray data, signed linear fold changes were used (e.g., +2 = twofold higher in FXR1 KD or OE than in control; −2 = twofold lower in FXR1 KD or OE than in control). Paired *t* tests (including replicate as a covariate) were performed for each gene between experimental groups to obtain a *t* statistic and *P* value for each gene. *t* statistics and nominal *P* values for each effect in the two-factor linear model, and *t* statistics and nominal *P* values for each pairwise comparison were generated. Benjamini-Hochberg false discovery rate (FDR) correction was applied across all genes to obtain FDR-corrected *P* values (FDR *q* values), which represent the probability that a given result is a false positive based on the distribution of all *P* values on the array. FDR *q* (filtered) values were recomputed separately for the two-factor model or each pairwise comparison, across only the genes that were expressed above the median value of at least as many samples as in

the smallest experimental group involved in the model/comparison. NES is normalized enrichment score for GSEA. For mass spectrometry data in other tables, SD, SEM, confidence interval (CI), *P* value derived by Student's *t* test, *P* value derived by *t* test with unequal variance, and *P* value derived by Welch's test were derived using Excel.

## SUPPLEMENTARY MATERIALS

Supplementary material for this article is available at https://science.org/doi/10.1126/sciadv.abo1304

View/request a protocol for this paper from *Bio-protocol*.

## REFERENCES AND NOTES


1. S. Lee, D. Micalizzi, S. S. Truesdell, S. I. A. Bukhari, M. Boukhali, J. Lombardi-Story, Y. Kato, M. K. Choo, I. Dey-Guha, F. Ji, B. T. Nicholson, D. T. Myers, D. Lee, M. A. Mazzola, R. Raheja, A. Langenbucher, N. J. Haradhvala, M. S. Lawrence, R. Gandhi, C. Tiedje, M. D. Diaz-Muñoz, D. A. Sweetser, R. Sadreyev, D. Sykes, W. Haas, D. A. Haber, S. Maheswaran, S. Vasudevan, A post-transcriptional program of chemoresistance by AU-rich elements and TTP in quiescent leukemic cells. *Genome Biol.* **21**, 33 (2020).
2. P. B. Gupta, T. T. onder, G. Jiang, K. Tao, C. Kuperwasser, R. A. Weinberg, E. S. Lander, Identification of selective inhibitors of cancer stem cells by high-throughput screening. *Cell* **138**, 645–659 (2009).
3. N. Sonenberg, A. G. Hinnebusch, Regulation of translation initiation in eukaryotes: Mechanisms and biological targets. *Cell* **136**, 731–745 (2009).
4. M. Costa-Mattioli, P. Walter, The integrated stress response: From mechanism to disease. *Science* **368**, eaat5314 (2020).
5. M. L. Truitt, D. Ruggero, New frontiers in translational control of the cancer genome. *Nat. Rev. Cancer* **16**, 288–304 (2016).
6. H. P. Harding, Y. Zhang, H. Zeng, I. Novoa, P. D. Lu, M. Calfon, N. Sadri, C. Yun, B. Popko, R. Paules, D. F. Stojdl, J. C. Bell, T. Hettmann, J. M. Leiden, D. Ron, An integrated stress response regulates amino acid metabolism and resistance to oxidative stress. *Mol. Cell* **11**, 619–633 (2003).
7. M. C. Siomi, Y. Zhang, H. Siomi, G. Dreyfuss, Specific sequences in the fragile X syndrome protein FMR1 and the FXR proteins mediate their binding to 60S ribosomal subunits and the interactions among them. *Mol. Cell. Biol.* **16**, 3825–3832 (1996).
8. R. Mazroui, M. E. Huot, S. Tremblay, C. Filion, Y. Labelle, E. W. Khandjian, Trapping of messenger RNA by Fragile X Mental Retardation protein into cytoplasmic granules induces translation repression. *Hum. Mol. Genet.* **11**, 3007–3017 (2002).
9. J. Qian, M. Hassanein, M. D. Hoeksema, B. K. Harris, Y. Zou, H. Chen, P. Lu, R. Eisenberg, J. Wang, A. Espinosa, X. Ji, F. T. Harris, S. M. J. Rahman, P. P. Massion, The RNA binding protein FXR1 is a new driver in the 3q26-29 amplicon and predicts poor prognosis in human cancers. *Proc. Natl. Acad. Sci. U.S.A.* **112**, 3469–3474 (2015).
10. S. I. Bukhari, S. S. Truesdell, S. Lee, S. Kollu, A. Classon, M. Boukhali, E. Jain, R. D. Mortensen, A. Yanagiya, R. I. Sadreyev, W. Haas, S. Vasudevan, A specialized mechanism of translation mediated by FXR1a-associated microRNP in cellular quiescence. *Mol. Cell* **61**, 760–773 (2016).
11. O. Le Tonqueze, S. Kollu, S. Lee, M. Al-Salah, S. S. Truesdell, S. Vasudevan, Regulation of monocyte induced cell migration by the RNA binding protein, FXR1. *Cell Cycle* **15**, 1874–1882 (2016).
12. L. I. Shlush, S. Zandi, A. Mitchell, W. C. Chen, J. M. Brandwein, V. Gupta, J. A. Kennedy, A. D. Schimmer, A. C. Schuh, K. W. Yee, J. L. Mc Leod, M. Doedens, J. J. F. Medeiros, R. Marke, H. J. Kim, K. Lee, J. D. McPherson, T. J. Hudson; HALT Pan-Leukemia Gene Panel Consortium, A. M. K. Brown, F. Yousif, Q. M. Trinh, L. D. Stein, M. D. Minden, J. C. Y. Wang, J. E. Dick, Identification of pre-leukaemic haematopoietic stem cells in acute leukaemia. *Nature* **506**, 328–333 (2014).
13. D. J. DeAngelo, E. M. Stein, F. Ravandi, Evolving therapies in acute myeloid leukemia: Progress at last? *Am. Soc. Clin. Oncol. Educ. Book* **35**, e302-12 (2016).
14. S. Lee, S. S. Truesdell, S. I. Bukhari, J. H. Lee, O. LeTonqueze, S. Vasudevan, Upregulation of eIF5B controls cell-cycle arrest and specific developmental stages. *Proc. Natl. Acad. Sci. U.S.A.* **111**, E4315–E4322 (2014).
15. D. L. J. Lafontaine, Noncoding RNAs in eukaryotic ribosome biogenesis and function. *Nat. Struct. Mol. Biol.* **22**, 11–19 (2015).
16. K. E. Sloan, A. S. Warda, S. Sharma, K. D. Entian, D. L. J. Lafontaine, M. T. Bohnsack, Tuning the ribosome: The influence of rRNA modification on eukaryotic ribosome biogenesis and function. *RNA Biol.* **14**, 1138–1152 (2017).
17. S. O. Sulima, I. J. F. Hofman, K. De Keersmaecker, J. D. Dinman, How ribosomes translate cancer. *Cancer Discov.* **7**, 1069–1087 (2017).
18. J. Baßler, E. Hurt, Eukaryotic ribosome assembly. *Annu. Rev. Biochem.* **88**, 281–306 (2019).
19. M. S. Scott, M. Ono, K. Yamada, A. Endo, G. J. Barton, A. I. Lamond, Human box C/D snoRNA processing conservation across multiple cell types. *Nucleic Acids Res.* **40**, 3676–3688 (2012).
20. J. Gong, Y. Li, C. J. Liu, Y. Xiang, C. Li, Y. Ye, Z. Zhang, D. H. Hawke, P. K. Park, L. Diao, J. A. Putkey, L. Yang, A. Y. Guo, C. Lin, L. Han, A pan-cancer analysis of the expression and clinical relevance of small nucleolar RNAs in human cancer. *Cell Rep.* **21**, 1968–1981 (2017).
21. Y. Motorin, V. Marchand, Detection and analysis of RNA ribose 2'-*O*-methylations: Challenges and solutions. *Genes* **9**, 642 (2018).
22. N. Krogh, M. D. Jansson, S. J. Häfner, D. Tehler, U. Birkedal, M. Christensen-Dalsgaard, A. H. Lund, H. Nielsen, Profiling of 2'-O-Me in human rRNA reveals a subset of fractionally modified positions and provides evidence for ribosome heterogeneity. *Nucleic Acids Res.* **44**, 7884–7895 (2016).
23. T. Kiss, B. E. Jady, Functional characterization of 2'-O-methylation and pseudouridylation guide RNAs. *Methods Mol. Biol.* **265**, 393–408 (2004).
24. V. Marcel, S. E. Ghayad, S. Belin, G. Therizols, A.-P. Morel, E. Solano-Gonzàlez, J. A. Vendrell, S. Hacot, H. C. Mertani, M. A. Albaret, J.-C. Bourdon, L. Jordan, A. Thompson, Y. Tafer, R. Cong, P. Bouvet, J.-C. Saurin, F. Catez, A.-C. Prats, A. Puisieux, J.-J. Diaz, p53 acts as a safeguard of translational control by regulating fibrillarin and rRNA methylation in cancer. *Cancer Cell* **24**, 318–330 (2013).
25. H. Khatter, A. G. Myasnikov, S. K. Natchiar, B. P. Klaholz, Structure of the human 80S ribosome. *Nature* **520**, 640–645 (2015).
26. S. K. Natchiar, A. G. Myasnikov, H. Kratzat, I. Hazemann, B. P. Klaholz, Visualization of chemical modifications in the human 80S ribosome structure. *Nature* **551**, 472–477 (2017).
27. V. Marcel, J. Kielbassa, V. Marchand, K. S. Natchiar, H. Paraqindes, F. N. Van Long, L. Ayadi, V. Bourguignon-Igel, P. L. Monaco, D. Monchiet, V. Scott, L. Tonon, S. E. Bray, A. Diot, L. B. Jordan, A. M. Thompson, J.-C. Bourdon, T. Dubois, F. André, F. Catez, A. Puisieux, Y. Motorin, B. P. Klaholz, A. Viari, J.-J. Diaz, Ribosomal RNA 2'O-methylation as a novel layer of inter-tumour heterogeneity in breast cancer. *NAR Cancer* **2**, zcaa036 (2020).
28. A. M. Anger, J. P. Armache, O. Berninghausen, M. Habeck, M. Subklewe, D. N. Wilson, R. Beckmann, Structures of the human and Drosophila 80S ribosome. *Nature* **497**, 80–85 (2013).
29. S. Klinge, F. Voigts-Hoffmann, M. Leibundgut, N. Ban, Atomic structures of the eukaryotic ribosome. *Trends Biochem. Sci.* **37**, 189–198 (2012).
30. N. J. Watkins, I. Lemm, D. Ingelfinger, C. Schneider, M. Hoßbach, H. Urlaub, R. Lührmann, Assembly and maturation of the U3 snoRNP in the nucleoplasm in a large dynamic multiprotein complex. *Mol. Cell* **16**, 789–798 (2004).
31. B. Renvoisé, S. Colasse, P. Burlet, L. Viollet, U. T. Meier, S. Lefebvre, The loss of the snoRNP chaperone Nopp140 from Cajal bodies of patient fibroblasts correlates with the severity of spinal muscular atrophy. *Hum. Mol. Genet.* **18**, 1181–1189 (2009).
32. E. Calo, B. Gu, M. E. Bowen, F. Aryan, A. Zalc, J. Liang, R. A. Flynn, T. Swigut, H. Y. Chang, L. D. Attardi, J. Wysocka, Tissue-selective effects of nucleolar stress and rDNA damage in developmental disorders. *Nature* **554**, 112–117 (2018).
33. F. Zhou, Y. Liu, C. Rohde, C. Pauli, D. Gerloff, M. Köhn, D. Misiak, N. Bäumer, C. Cui, S. Göllner, T. Oellerich, H. Serve, M. P. Garcia-Cuellar, R. Slany, J. P. Maciejewski, B. Przychodzen, B. Seliger, H. U. Klein, C. Bartenhagen, W. E. Berdel, M. Dugas, M. M. Taketo, D. Farouq, S. Schwartz, A. Regev, J. Hébert, G. Sauvageau, C. Pabst, S. Hüttelmaier, C. Müller-Tidow, AML1-ETO requires enhanced C/D box snoRNA/RNP formation to induce self-renewal and leukaemia. *Nat. Cell Biol.* **19**, 844–855 (2017).
34. E. Calo, R. A. Flynn, L. Martin, R. C. Spitale, H. Y. Chang, J. Wysocka, RNA helicase DDX21 coordinates transcription and ribosomal RNA processing. *Nature* **518**, 249–253 (2015).
35. J. George, Y. Li, I. P. Kadamberi, D. Parashar, S. W. Tsaih, P. Gupta, A. Geethadevi, C. Chen, C. Ghosh, Y. Sun, S. Mittal, R. Ramchandran, H. Rui, G. Lopez-Berestein, C. Rodriguez-Aguayo, G. Leone, J. S. Rader, A. K. Sood, M. Dey, S. Pradeep, P. Chaluvally-Raghavan, RNA-binding protein FXR1 drives cMYC translation by recruiting eIF4F complex to the translation start site. *Cell Rep.* **37**, 109934 (2021).
36. J. van Riggelen, A. Yetil, D. W. Felsher, MYC as a regulator of ribosome biogenesis and protein synthesis. *Nat. Rev. Cancer* **10**, 301–309 (2010).
37. N. R. Genuth, M. Barna, The discovery of ribosome heterogeneity and its implications for gene regulation and organismal life. *Mol. Cell* **71**, 364–374 (2018).
38. E. A. Lerner, M. R. Lerner, C. A. Janeway Jr., J. A. Steitz, Monoclonal antibodies to nucleic acid-containing cellular constituents: Probes for molecular biology and autoimmune disease. *Proc. Natl. Acad. Sci. U.S.A.* **78**, 2737–2741 (1981).
39. A. J. Inglis, G. R. Masson, S. Shao, O. Perisic, S. H. McLaughlin, R. S. Hegde, R. L. Williams, Activation of GCN2 by the ribosomal P-stalk. *Proc. Natl. Acad. Sci. U.S.A.* **116**, 4946–4954 (2019).
40. H. P. Harding, A. Ordonez, F. Allen, L. Parts, A. J. Inglis, R. L. Williams, D. Ron, The ribosomal P-stalk couples amino acid starvation to GCN2 activation in mammalian cells. *eLife* **8**, e50149 (2019).
41. C. C. Wu, A. Peterson, B. Zinshteyn, S. Regot, R. Green, Ribosome collisions trigger general stress responses to regulate cell fate. *Cell* **182**, 404–416.e14 (2020).
42. L. Wan, S. Juszkiewicz, D. Blears, P. K. Bajpe, Z. Han, P. Faull, R. Mitter, A. Stewart, A. P. Snijders, R. S. Hegde, J. Q. Svejstrup, Translation stress and collided ribosomes are co-activators of cGAS. *Mol. Cell* **81**, 2808–2822.e10 (2021).

43. R. Toroney, C. M. Hull, J. E. Sokoloski, P. C. Bevilacqua, Mechanistic characterization of the 5′-triphosphate-dependent activation of PKR: Lack of 5′-end nucleobase specificity, evidence for a distinct triphosphate binding site, and a critical role for the dsRBD. *RNA* **18**, 1862–1874 (2012).
44. O. A. Youssef, S. A. Safran, T. Nakamura, D. A. Nix, G. S. Hotamisligil, B. L. Bass, Potential role for snoRNAs in PKR activation during metabolic stress. *Proc. Natl. Acad. Sci. U.S.A.* **112**, 5023–5028 (2015).
45. V. Gandin, L. Masvidal, M. Cargnello, L. Gyenis, S. McLaughlan, Y. Cai, C. Tenkerian, M. Morita, P. Balanathan, O. Jean-Jean, V. Stambolic, M. Trost, L. Furic, L. Larose, A. E. Koromilas, K. Asano, D. Litchfield, O. Larsson, I. Topisirovic, mTORC1 and CK2 coordinate ternary and eIF4F complex assembly. *Nat. Commun.* **7**, 11127 (2016).
46. K. A. Spriggs, M. Stoneley, M. Bushell, A. E. Willis, Re-programming of translation following cell stress allows IRES-mediated translation to predominate. *Biol. Cell* **100**, 27–38 (2008).
47. M. G. Kearse, J. E. Wilusz, Non-AUG translation: A new start for protein synthesis in eukaryotes. *Genes Dev.* **31**, 1717–1731 (2017).
48. I. P. Ivanov, A. E. Firth, A. M. Michel, J. F. Atkins, P. V. Baranov, Identification of evolutionarily conserved non-AUG-initiated N-terminal extensions in human coding sequences. *Nucleic Acids Res.* **39**, 4220–4234 (2011).
49. M. G. Cardenas, W. Yu, W. Beguelin, M. R. Teater, H. Geng, R. L. Goldstein, E. Oswald, K. Hatzi, S. N. Yang, J. Cohen, R. Shaknovich, K. Vanommeslaeghe, H. Cheng, D. Liang, H. J. Cho, J. Abbott, W. Tam, W. du, J. P. Leonard, O. Elemento, L. Cerchietti, T. Cierpicki, F. Xue, A. D. MacKerell Jr., A. M. Melnick, Rationally designed BCL6 inhibitors target activated B cell diffuse large B cell lymphoma. *J. Clin. Invest.* **126**, 3351–3362 (2016).
50. R. Majeti, M. P. Chao, A. A. Alizadeh, W. W. Pang, S. Jaiswal, K. D. Gibbs Jr., N. van Rooijen, I. L. Weissman, CD47 is an adverse prognostic factor and therapeutic antibody target on human acute myeloid leukemia stem cells. *Cell* **138**, 286–299 (2009).
51. A. Khateb, Z. A. Ronai, Unfolded protein response in leukemia: From basic understanding to therapeutic opportunities. *Trends Cancer* **6**, 960–973 (2020).
52. C. Bergom, R. Goel, C. Paddock, C. Gao, D. K. Newman, S. Matsuyama, P. J. Newman, The cell-adhesion and signaling molecule PECAM-1 is a molecular mediator of resistance to genotoxic chemotherapy. *Cancer Biol. Ther.* **5**, 1699–1707 (2006).
53. L. Cui, Z. Cheng, Y. Liu, Y. Dai, Y. Pang, Y. Jiao, X. Ke, W. Cui, Q. Zhang, J. Shi, L. Fu, Overexpression of PDK2 and PDK3 reflects poor prognosis in acute myeloid leukemia. *Cancer Gene Ther.* **27**, 15–21 (2020).
54. G. W. Byeon, E. S. Cenik, L. Jiang, H. Tang, R. das, M. Barna, Functional and structural basis of extreme conservation in vertebrate 5′ untranslated regions. *Nat. Genet.* **53**, 729–741 (2021).
55. A. Sendoel, J. G. Dunn, E. H. Rodriguez, S. Naik, N. C. Gomez, B. Hurwitz, J. Levorse, B. D. Dill, D. Schramek, H. Molina, J. S. Weissman, E. Fuchs, Translation from unconventional 5′ start sites drives tumour initiation. *Nature* **541**, 494–499 (2017).
56. K. Pakos-Zebrucka, I. Koryga, K. Mnich, M. Ljujic, A. Samali, A. M. Gorman, The integrated stress response. *EMBO Rep.* **17**, 1374–1395 (2016).
57. R. Ishimura, G. Nagy, I. Dotu, J. H. Chuang, S. L. Ackerman, Activation of GCN2 kinase by ribosome stalling links translation elongation with translation initiation. *eLife* **5**, e14295 (2016).
58. S. K. Young, L. R. Palam, C. Wu, M. S. Sachs, R. C. Wek, Ribosome elongation stall directs gene-specific translation in the integrated stress response. *J. Biol. Chem.* **291**, 6546–6558 (2016).
59. J. Visweswaraiah, S. Lageix, B. A. Castilho, L. Izotova, T. G. Kinzy, A. G. Hinnebusch, E. Sattlegger, Evidence that eukaryotic translation elongation factor 1A (eEF1A) binds the Gcn2 protein C terminus and inhibits Gcn2 activity. *J. Biol. Chem.* **286**, 36568–36579 (2011).
60. J. C. Darnell, S. J. van Driesche, C. Zhang, K. Y. S. Hung, A. Mele, C. E. Fraser, E. F. Stone, C. Chen, J. J. Fak, S. W. Chi, D. D. Licatalosi, J. D. Richter, R. B. Darnell, FMRP stalls ribosomal translocation on mRNAs linked to synaptic function and autism. *Cell* **146**, 247–261 (2011).
61. R. J. Argüello, M. Reverendo, A. Mendes, V. Camosseto, A. G. Torres, L. R. de Pouplana, S. A. van de Pavert, E. Gatti, P. Pierre, SunRiSE - Measuring translation elongation at single-cell resolution by means of flow cytometry. *J. Cell Sci.* **131**, jcs214346 (2018).
62. S. Stark, C. Watzl, 2B4 (CD244), NTB-A and CRACC (CS1) stimulate cytotoxicity but no proliferation in human NK cells. *Int. Immunol.* **18**, 241–247 (2006).
63. A. F. Zyryanova, K. Kashiwagi, C. Rato, H. P. Harding, A. Crespillo-Casado, L. A. Perera, A. Sakamoto, M. Nishimoto, M. Yonemochi, M. Shirouzu, T. Ito, D. Ron, ISRIB blunts the integrated stress response by allosterically antagonising the inhibitory effect of phosphorylated eIF2 on eIF2B. *Mol. Cell* **81**, 88–103.e6 (2021).
64. C. Lebeaupin, J. Yong, R. J. Kaufman, The impact of the ER unfolded protein response on cancer initiation and progression: Therapeutic implications. *Adv. Exp. Med. Biol.* **1243**, 113–131 (2020).
65. M. Ri, E. Tashiro, D. Oikawa, S. Shinjo, M. Tokuda, Y. Yokouchi, T. Narita, A. Masaki, A. Ito, J. Ding, S. Kusumoto, T. Ishida, H. Komatsu, Y. Shiotsu, R. Ueda, T. Iwawaki, M. Imoto, S. Iida, Identification of Toyocamycin, an agent cytotoxic for multiple myeloma cells, as a potent inhibitor of ER stress-induced XBP1 mRNA splicing. *Blood Cancer J.* **2**, e79 (2012).
66. L. L. Yan, H. S. Zaher, Ribosome quality control antagonizes the activation of the integrated stress response on colliding ribosomes. *Mol. Cell* **81**, 614–628.e4 (2021).
67. S. Meydan, N. R. Guydosh, A cellular handbook for collided ribosomes: Surveillance pathways and collision types. *Curr. Genet.* **67**, 19–26 (2021).
68. B. J. Guan, V. van Hoef, R. Jobava, O. Elroy-Stein, L. S. Valasek, M. Cargnello, X.-H. Gao, D. Krokowski, W. C. Merrick, S. R. Kimball, A. A. Komar, A. E. Koromilas, A. Wynshaw-Boris, I. Topisirovic, O. Larsson, M. Hatzoglou, A unique ISR program determines cellular responses to chronic stress. *Mol. Cell* **68**, 885–900.e6 (2017).
69. E. Boye, B. Grallert, eIF2α phosphorylation and the regulation of translation. *Curr. Genet.* **66**, 293–297 (2020).
70. E. G. Bechara, M. C. Didiot, M. Melko, L. Davidovic, M. Bensaid, P. Martin, M. Castets, P. Pognonec, E. W. Khandjian, H. Moine, B. Bardoni, A novel function for fragile X mental retardation protein in translational activation. *PLOS Biol.* **7**, e16 (2009).
71. Y. H. Xing, R.-W. Yao, Y. Zhang, C.-J. Guo, S. Jiang, G. Xu, R. Dong, L. Yang, L.-L. Chen, SLERT regulates DDX21 rings associated with Pol I transcription. *Cell* **169**, 664–678.e16 (2017).
72. M. G. Kearse, D. H. Goldman, J. Choi, C. Nwaezeapu, D. Liang, K. M. Green, A. C. Goldstrohm, P. K. Todd, R. Green, J. E. Wilusz, Ribosome queuing enables non-AUG translation to be resistant to multiple protein synthesis inhibitors. *Genes Dev.* **33**, 871–885 (2019).
73. D. W. Huang, B. T. Sherman, R. A. Lempicki, Bioinformatics enrichment tools: Paths toward the comprehensive functional analysis of large gene lists. *Nucleic Acids Res.* **37**, 1–13 (2009).
74. A. Subramanian, P. Tamayo, V. K. Mootha, S. Mukherjee, B. L. Ebert, M. A. Gillette, A. Paulovich, S. L. Pomeroy, T. R. Golub, E. S. Lander, J. P. Mesirov, Gene set enrichment analysis: A knowledge-based approach for interpreting genome-wide expression profiles. *Proc. Natl. Acad. Sci. U.S.A.* **102**, 15545–15550 (2005).
75. P. Ruytinx, P. Proost, J. Van Damme, S. Struyf, Chemokine-induced macrophage polarization in inflammatory conditions. *Front. Immunol.* **9**, (2018).
76. C. A. Hoy, L. C. Seamer, R. T. Schimke, Thermal denaturation of DNA for immunochemical staining of incorporated bromodeoxyuridine (BrdUrd): Critical factors that affect the amount of fluorescence and the shape of BrdUrd/DNA histogram. *Cytometry* **10**, 718–725 (1989).
77. K. Kojima, M. Konopleva, I. J. Samudio, M. Shikami, M. Cabreira-Hansen, T. McQueen, V. Ruvolo, T. Tsao, Z. Zeng, L. T. Vassilev, M. Andreeff, MDM2 antagonists induce p53-dependent apoptosis in AML: Implications for leukemia therapy. *Blood* **106**, 3150–3159 (2005).
78. T. L. Bailey, C. Elkan, Fitting a mixture model by expectation maximization to discover motifs in biopolymers. *Proc. Int. Conf. Intell. Syst. Mol. Biol.* **2**, 28–36 (1994).
79. R. Lorenz, S. H. Bernhart, C. HönerZuSiederdissen, H. Tafer, C. Flamm, P. F. Stadler, I. L. Hofacker, ViennaRNA Package 2.0. *Algorithms Mol. Biol.* **6**, 26 (2011).


**Acknowledgments:** We thank D. Scadden and D. Sykes for cell lines and C. P. de Leon for technical support, HSCI-CRM Flow-Cytometry facility at MGH for flow cytometry, Partners Health Care Center for Personalized Genetic Medicine and BUMC facilities for microarray data, and Arraystar for LC-MS modification data. **Funding:** The study is funded by GM134944 and CA220103 grants from the NIH and a Kurt Isselbacher grant from the RICBAC Foundation to S.V. **Author contributions:** C.D. conducted the research. S.S.T., K.Q.W., S.I.A.B., H.N., B.B., O.L.T., S.L., S.K., M.A.G., M.S.B., and L.B. contributed to the data. M.B., J.K., and W.H. conducted proteomics. S.V. supervised the project and wrote the manuscript. **Competing interests:** The authors declare that they have no competing interests. A provisional patent was filed on this study on 15 October 2021 by MGH (S.V., C.D., and S.S.T. as authors, #2022-015). **Data and materials availability:** All data are present in the paper and as attached supplementary tables (excel spreadsheets). Microarray cel files are publicly available at GEO (GSE211932 and GSE211933).

Submitted 19 January 2022
Accepted 8 September 2022
Published 28 October 2022
10.1126/sciadv.abo1304